Overexpression of peroxisome proliferator-activated receptor γ co-activator-1 α (PGC-1 α) in Chinese hamster ovary cells increases oxidative metabolism and IgG productivity

Sarah A. Sacco^{1, ‡}, Allison G. McAtee Pereira^{1, ‡}, Irina Trenary¹, Kevin D. Smith^{2, †}, Michael J. Betenbaugh³, Jamey D. Young^{1,*}

¹Department of Chemical and Biomolecular Engineering, Vanderbilt University, Nashville, TN, USA

²Pharmaceutical Development and Manufacturing Sciences, Janssen Research and Development, Spring House, PA, USA

³Department of Chemical and Biomolecular Engineering, Johns Hopkins University, Baltimore, MD, USA

[†]Current address: Asimov, 201 Brookline Ave., Boston, MA

[‡]These authors contributed equally to this work

*Corresponding author

To whom correspondence should be addressed:

Jamey D. Young PMB 351604

Nashville, TN 37235-1604

Email: j.d.young@vanderbilt.edu

ABSTRACT

Chinese hamster ovary (CHO) cells are used extensively to produce protein therapeutics, such as monoclonal antibodies (mAbs), in the biopharmaceutical industry. MAbs are large proteins that are energetically demanding to synthesize and secrete; therefore, high-producing CHO cell lines that are engineered for maximum metabolic efficiency are needed to meet increasing demands for mAb production. Previous studies have identified that high-producing cell lines possess a distinct metabolic phenotype when compared to low-producing cell lines. In particular, it was found that high mAb production is correlated to lactate consumption and elevated TCA cycle flux. We hypothesized that enhancing flux through the mitochondrial TCA cycle and oxidative phosphorylation would lead to increased mAb productivities and final titers. To test this hypothesis, we overexpressed peroxisome proliferator-activated receptor γ co-activator-1 α (PGC-1 α), a gene that promotes mitochondrial metabolism, in an IgG-producing parental CHO cell line. Stable cell pools overexpressing PGC-1α exhibited increased oxygen consumption, indicating increased mitochondrial metabolism, as well as increased mAb specific productivity compared to the parental line. We also performed ¹³C metabolic flux analysis (MFA) to quantify how PGC-1α overexpression alters intracellular metabolic fluxes, revealing not only increased TCA cycle flux, but global upregulation of cellular metabolic activity. This study demonstrates the potential of rationally engineering the metabolism of industrial cell lines to improve overall mAb productivity and to increase the abundance of highproducing clones in stable cell pools.

1 Introduction

Monoclonal antibodies (mAbs) represent the largest class of biopharmaceuticals, accounting for over 50% of new drug approvals and 65% of global biopharmaceutical sales (Walsh, 2018). MAbs bind their target antigens with high specificity, leading to less side effects during treatment, and are currently used as therapies against a wide range of diseases such as autoimmune disorders, various cancers, and inflammatory diseases. Biopharmaceuticals are typically produced in mammalian cells due to the complexity of these macromolecule drugs. Chinese hamster ovary (CHO) cells are one of the most common mammalian host cell lines, used in the production of over 80% of recently approved mAbs (Walsh, 2018). CHO cells have the ability to perform human-like post-translational modifications that are necessary for the in vivo efficacy of most protein therapeutics (Majewska et al., 2020; Mcatee et al., 2014), can grow in serum-free media (Rodrigues et al., 2013; Schröder et al., 2004; Sinacore et al., 2000), and can be cultured in suspension (Becker et al., 2011; Fischer et al., 2015), all of which contribute to their preferential use in industry. While prior improvements in mAb production have been achieved through optimization of media formulations and bioprocess parameters, little progress has been made toward engineering host cell metabolism to increase the specific production rate (qP) of the mAb product (Jayapal et al., 2007; Kuo et al., 2018; Templeton et al., 2017a). With increasing demands and high dosage requirements for mAb treatments, there is a critical need to maximize productivity of mammalian cell cultures by enhancing the metabolic capabilities of CHO host lines.

Proteins are energetically expensive for cells to synthesize, requiring three ATP equivalents to form each peptide bond (Seth et al., 2006). During periods of high production, a recombinant mAb protein can represent up to 20% of total cellular protein synthesis. Additional ATP is required to package and secrete mAbs into the extracellular medium (Gutierrez et al., 2020). Despite the elevated demands for energy and biosynthetic precursors to produce mAbs at high yield, CHO cells often exhibit an inefficient central carbon metabolism. They typically consume excess nutrients (e.g., glucose and amino acids) and accumulate waste products such as lactate, ammonia, and other byproducts that inhibit cell growth and affect final product quality (Dorai et al., 2009; Lao and Toth, 1997; Le et al., 2012; Mulukutla et al., 2019). We previously reported that peak qP occurs during the stationary growth phase, coinciding with a switch to lactate consumption that supplies increased flux through oxidative metabolic pathways, particularly the mitochondrial TCA cycle (Templeton et al., 2013;

Templeton and Young, 2018). In a subsequent study, we found that high-producing CHO cell cultures consistently exhibited enhanced mitochondrial metabolism compared to low- or non-producing cultures across a panel of industrial CHO host lines (Templeton et al., 2017a). Based on these observations, we hypothesized that enhancing flux through the TCA cycle would lead to increased mAb productivity and higher final product titer.

To promote higher TCA cycle flux, we engineered an industrial IgG-expressing CHO cell line to overexpress peroxisome proliferator-activated receptor γ co-activator-1 α (PGC-1 α), a transcriptional coactivator that regulates oxidative metabolism in animal cells (**Fig. 1**) (Austin and St-Pierre, 2012; Chan and Arany, 2014; Puigserver and Spiegelman, 2003; Rodgers et al., 2008; Scarpulla, 2011). The role of PGC-1 α has been well studied in various cell types and tissues, such as cardiomyocytes, skeletal muscle, and liver (Chan and Arany, 2014; Lehman et al., 2000; Matthew Morris et al., 2012; Mootha et al., 2004). However, to the best of our knowledge, the overexpression of PGC-1 α has not been studied in CHO cells. In other cell types, overexpression of PGC-1 α increases oxygen consumption, mitochondrial biogenesis, and mitochondrial energy metabolism by activating transcription of downstream genes involved in mitochondrial substrate oxidation and ATP production (Chan and Arany, 2014; Lehman et al., 2000; Matthew Morris et al., 2012; Mootha et al., 2004). We therefore hypothesized that overexpression of PGC-1 α in the parental CHO cell line would lead to increased TCA cycle flux and therefore increased qP as a result of enhancing ATP supply and reducing waste product accumulation.

We applied 13 C metabolic flux analysis (MFA) to quantify the metabolic changes that occurred due to PGC-1 α overexpression by comparing the parental CHO host line with stable pools transfected with a PGC-1 α expression vector. By feeding 13 C-labeled glucose during stationary phase and measuring the isotopic enrichment of intracellular metabolites, fluxes through central carbon metabolism were quantified using a mathematical model of CHO central carbon metabolism (Antoniewicz, 2020; Sacco and Young, 2021). Because isotopic steady state was not achieved prior to the onset of death phase, isotopically nonstationary metabolic flux analysis (INST-MFA) was used to assess metabolism during stationary phase (Cheah and Young, 2018). TCA cycle flux was increased 3-fold in stable pools overexpressing PGC-1 α , which was

corroborated by independent measurements of oxygen uptake rate that showed a 2.4-fold elevation in cellular respiration. These increases in oxidative metabolism were associated with a 5.2-fold increase in qP relative to the parental line, lending support to the hypothesis that engineering mitochondrial energy-producing pathways can promote higher mAb productivity in CHO cell lines.

2 Materials and Methods

2.1 Generation of cell lines

An industrial IgG-producing CHO cell line, provided by Janssen, was used for this study. The pcDNA4-myc-PGC-1α plasmid was a gift from Toren Finkel (Addgene plasmid #10974; http://n2t.net/addgene:10974; RRID:Addgene 10974) (Ichida et al., 2002). The plasmid contains the coding sequence for human PGC-1α under a CMV promoter with Myc and His tags on the C-terminus and a zeocin resistance marker. Two days preceding transfection with the PGC-1α vector, cells were seeded at 2x10⁵ cells/mL in 50 mL fresh chemicallydefined Janssen proprietary medium (SAFC; Burlington, MA) in 125-mL shake flasks at 37°C, 5% CO₂, and shaking at 135 RPM. Since the mAb product was expressed via the glutamine synthetase (GS) expression system, methionine sulfoximine (MSX) was added to the medium to inhibit endogenous GS activity. On the day of transfection, cells were seeded in T-25 flasks containing 1x10⁷ live cells in 1 mL fresh medium containing 25 μM MSX. Then, 15 μg of purified PGC-1α expression vector DNA was incubated in 1.8 mL MSX-containing medium. Meanwhile, 37.5 µL polyethyleneimine (PEI) was separately incubated in 1.8 mL MSX-containing medium. The PEI solution was combined with the vector DNA aliquot and mixed thoroughly. The DNA/PEI mixture was incubated for 15 min at room temperature and then added to the T-25 flask containing the parental cells. Cells were incubated for 48 hours, then harvested, centrifuged at 1000 RPM (300 rcf) for five minutes, and the transfection medium was aspirated. The transfected cells were re-suspended in fresh medium containing MSX, 0.2%v/v phenol red, and 300 µg/mL zeocin (Invitrogen; Carlsbad, CA) at a density of 1.6x10⁴ cells per 200 µL. Phenol red (Sigma) was added for visual assessment of cell growth, while zeocin was added for antibiotic selection to inhibit growth of cells that did not integrate the PGC-1α DNA construct. The cell suspension was aliquoted into 96-well plates (200 µL/well) for stable mini-pool selection.

Roughly half of the medium in each well was removed via aspiration every three to four days and replaced with fresh growth medium. When the medium color change indicated rapid cell growth, the cells in those wells were expanded into 24-well plates, then to 12- and 6-well plates before being transferred to T-25 and then T-75 flasks. Once the expanded mini-pools reached sufficiently high cell densities, they were seeded at $3x10^5$ cells/mL in 30 mL medium and grown in 125-mL shake flasks as stable populations. The expanded stable pools were then characterized to verify successful transfection and expression of PGC-1 α .

2.2 Total RNA isolation and reverse transcriptase quantitative real-time PCR (RT-qPCR)

Total RNA was isolated from cells using the RNeasy Mini Kit (Qiagen; Germantown, MD) according to the manufacturer's protocol. Isolated RNA was reverse transcribed to cDNA using an iScript Reverse Transcription kit, according to the manufacturer's protocol (BioRad, Hercules, CA). Reactions without reverse transcriptase were run in parallel to assess DNA contamination. Quantitative real-time PCR (RT-qPCR) was performed on a BioRad CFX96 Cycler (BioRad, Hercules, CA) with 20- μ L reactions containing 25 ng/well of cDNA, 250 nm forward and reverse primers (**Table S1**), and 10 μ L SYBR Green PCR Master Mix (BioRad, Hercules, CA). Reactions were run for 40 cycles, and the threshold cycle (Ct) was determined from amplification curves using the CFX Maestro software (BioRad, Hercules, CA). Target gene expression was normalized to the expression of hypoxanthine-guanine phosphoribosyltransferase (HPRT), a housekeeping gene that has previously been used in CHO cells (Ko et al., 2018) and in other cell types where PGC-1 α expression was manipulated (Carrier et al., 2004; Lustig et al., 2011). Data were analyzed using a modified $\Delta\Delta$ Ct method (Livak and Schmittgen, 2001); since no expression of PGC-1 α , recombinant or endogenous, was detected in the parental control line, values were reported as $2^{-\Delta Ct}$, where Δ Ct represents the difference in Ct for the gene of interest relative to the HPRT housekeeping gene.

2.3 Cell culture and isotope labeling experiment

The parental line and three PGC-1α expressing pools (pool 1, 2, and 3) were grown in 125-mL shake flasks at 37°C and 5% CO₂ while shaking at 135 RPM. Four replicate flasks of each line were expanded from a single culture and grown in parallel. The cells were cultivated in chemically-defined Janssen proprietary medium with 25 μM MSX and 300 μg/mL zeocin (Invitrogen) and proprietary feeds (Janssen) of amino acids and other nutrients added according to the timeline in **Table 1**. A bolus of 100% [U-¹³C₆]glucose was fed to two replicate flasks of each cell line at the start of stationary growth phase (day five of culture). The onset of stationary growth phase was designated as the point when lactate metabolism switched from production to consumption. The volume of the glucose bolus was adjusted so that 70% of the total glucose would be labeled after the ¹³C-glucose bolus was fed. Two additional replicate flasks were fed natural (i.e., unlabeled) glucose at this time. The unlabeled cultures were sampled daily to assess growth and extracellular exchange rates. After two days

of incubation with ¹³C-glucose, cell pellets were collected from the labeled cultures roughly every 12 hours and were immediately cold-quenched as described previously (Templeton et al., 2014).

2.4 Determination of growth and extracellular exchange rates

Culture viable cell densities (VCDs) and percent viabilities were measured using a trypan blue exclusion method with a Cedex XS automated counter (Roche, Basel, Switzerland). Medium amino acid concentrations were analyzed using an Agilent 1200 series high performance liquid chromatograph (HPLC) as described previously (Templeton et al., 2014). Medium glucose and lactate concentrations were measured using a YSI 2300 biochemical analyzer (YSI, Yellow Springs, OH), and mAb titers were measured with a ForteBio Octet RED96 (Pall, Menlo Park, CA). Net growth rates, death rates, and extracellular fluxes were calculated by the ETA software package (Murphy and Young, 2013) as previously described (Templeton et al., 2014).

2.5 Oxygen consumption measurements

Oxygen uptake rates (OURs) were measured using an Oroboros Oxygraph-2k instrument, which contains two chambers with separate oxygen probes to monitor on-line changes in oxygen concentration over time. The instrument was set to 37° C, and cells were harvested from each culture and re-suspended in growth medium at a density of $2x10^{6}$ cells/mL. For each PGC-1 α pool, two million cells were injected into one chamber of the instrument while two million cells of the parental control line were injected into the opposite chamber. The parental line was included in each experiment to control for chamber effects. The rates of oxygen consumption were allowed to reach equilibrium for a minimum of five minutes before OUR was measured.

2.6 Gas chromatography-mass spectrometry (GC-MS) measurements

Gas chromatography-mass spectrometry (GC-MS) was used to assess ¹³C enrichments of metabolites over the time course of the isotope labeling experiments. Intracellular metabolites were extracted from cold-quenched cell pellets, derivatized, and analyzed by GC-MS as described previously (Templeton et al., 2017a, 2013). GC-MS analysis of medium glucose was performed by di-*O*-isopropylidene derivatization to determine the enrichment of ¹³C-glucose in each labeled flask as previously described (Antoniewicz et al., 2011).

2.7 ¹³C isotopically non-stationary metabolic flux analysis (INST-MFA)

An isotopomer model was constructed based on a previously described CHO cell metabolic network to simulate the mass isotopomer distributions (MIDs) of intracellular metabolites following administration of the ¹³C-glucose tracer (Templeton et al., 2014). The model comprised 80 metabolic reactions, 22 extracellular metabolite exchange rates, and two macromolecular products (mAb and biomass) as detailed in **Tables S3-6**. Isotopomer models were regressed to fit the experimental data sets for each cell line using the INCA software package (Young, 2014), as previously described (Templeton et al., 2014). All model fits were overdetermined, and the best-fit flux solution was obtained from at least 50 independent trials, each starting from random initial guesses, in order to converge on a global optimum. (Best practices recommend at least 10 independent trials to ensure a global optimum solution (Antoniewicz, 2020; Crown and Antoniewicz, 2013).) Due to the lack of isotopic steady state measurements, INST-MFA was used to regress flux solutions for each cell line based on measurements collected between days 6-8 of culture. Goodness-of-fit metrics for each best-fit solution are provided in **Table S2**, and 95% confidence intervals were calculated for all flux parameters by evaluating the sensitivity of the sum-of-squared residuals to parameter variations (**Tables S3-6**). The Cytoscape software package was used to produce images of the resulting flux maps (Shannon et al., 2003).

2.8 Statistical analysis

Significant differences between fluxes of the different cell lines were analyzed via two-way ANOVA (α = 0.05) with Tukey-Kramer post-hoc testing. Standard errors of the mean (SEM) for each flux were calculated from 95% confidence bounds provided by INCA (i.e., by dividing the difference between the upper and lower bounds by 3.92).

3 Results

3.1 Generation and selection of stable PGC-1 α expressing pools

After transfection with the PGC-1 α expression vector, a total of 20 PGC-1 α stable cell lines were generated from the antibiotic-resistant mini-pools. Eight of the transfected lines exhibited loss of mAb expression due to the selection process and therefore were not studied further. The remaining twelve cell lines were evaluated based on the measured qP compared to the parental line and the expression level of recombinant PGC-1 α mRNA, as measured by RT-qPCR (**Fig. 2**). While ten of the twelve pools had qP values that trended higher than the parental line, three pools exhibited significantly higher qP levels compared to the parental line and mid-range mRNA overexpression of recombinant PGC-1 α . These three PGC-1 α overexpressing lines were selected for further characterization and are referred to herein as pools 1, 2, and 3. The qP of the other nine pools trended higher than the parental line but were not significantly elevated due to variability in the data and the low number of replicates used for this initial cell screening experiment.

3.2 Expression of recombinant and endogenous PGC-1α mRNA in stable pools

To confirm successful integration and expression of PGC-1 α in the three selected pools, mRNA levels of both recombinant (human) and endogenous (CHO) PGC-1 α were evaluated using RT-qPCR. Unique primer sets were used to independently quantify mRNA expression of each PGC-1 α isoform. On both days 5 and 7 of culture, high levels of recombinant PGC-1 α mRNA were detected in all three stable pools (**Fig. 3**). No recombinant PGC-1 α expression was detected in the parental line, implying there was no endogenous interference or non-specific binding of primers. Endogenous PGC-1 α mRNA levels were also evaluated to determine the extent to which they were altered by recombinant PGC-1 α expression, since PGC-1 α expression is autoregulatory (Amat et al., 2009; Handschin et al., 2003). Relatively low endogenous levels of PGC-1 α were detected on day 5 of culture in the three engineered pools, but expression increased over 100-fold by day 7 (**Fig. 3**). No endogenous expression of PGC-1 α was detected in the parental line, suggesting that recombinant expression of human PGC-1 α upregulated the expression of endogenous CHO PGC-1 α to detectable levels in the stable pools.

3.3 PGC-1 α expression attenuated growth but increased mAb specific productivity

VCD was measured daily over the course of the fed-batch experiment summarized in **Table 1**. Both the exponential growth rate and peak VCD were significantly lower in the PGC-1 α expressing pools compared to the parental line (**Fig. 4A, B**). This reduction in growth rate correlated with an increase in cell volume of ~50% on average (**Fig. S1**). The slower growth of the PGC-1 α pools was likely attributable to the increased metabolic burden of expressing recombinant PGC-1 α in addition to the mAb product. Furthermore, metabolic alterations arising from PGC-1 α expression may have limited cell growth. Despite this reduction in growth, volumetric titers of the three PGC-1 α pools were significantly higher (by 1.5- to 2-fold) compared to the parental line (**Fig. 4C,D**). The increased titers were due to significantly higher qP values that were nearly 4-fold greater than that of the parental line (**Fig. 4E**). Even when accounting for the increased size of PGC-1 α expressing cells, productivities were still higher when calculated on a per cell volume, rather than a per cell number, basis.

3.4 PGC-1 α expressing pools exhibit higher consumption of oxygen and carbon sources

Oxygen uptake rates (OURs) are typically elevated in cells and tissues that overexpress PGC-1 α , which serves as an indicator of increased oxidative metabolism (Lehman et al., 2000). OURs were measured for each PGC-1 α pool and compared to the parental line on the final day of the fed-batch experiment when the cultures were in stationary growth phase (**Table 1**). All pools exhibited significantly higher OURs compared to the parental line (**Fig. 5**). These results indicate that the PGC-1 α expressing pools exhibited substantial enhancements in oxidative metabolism during stationary phase. Supporting this observation, the consumption of several carbon sources was significantly higher in the PGC-1 α expressing pools. Glucose uptake rates during stationary phase were nearly doubled compared to the parental line, while lactate uptake rates were at least 4-fold higher in the PGC-1 α pools (**Fig. 6**). The increased consumption of these two major carbon sources likely fueled the increased oxidative metabolism of the PGC-1 α expressing pools. Additionally, the consumption of nine out of fifteen measured amino acids was significantly higher, while the production of alanine, glutamine, and glycine were all significantly enhanced by expression of PGC-1 α (**Fig. S2**).

3.5 13 C MFA reveals extensive upregulation of energy metabolism in PGC-1 α expressing pools

To further assess the intracellular metabolic alterations that underpinned the observed increases in OUR and substrate consumption rates in stable PGC-1 α pools, we applied ¹³C MFA to quantify metabolic pathway fluxes from isotope labeling datasets. Nearly all fluxes in glycolysis and the TCA cycle were elevated in the three PGC-1 α expressing pools compared to the parental line (**Fig. 7**). The model-determined increases in glycolytic fluxes were consistent with the directly measured increases in GUR (**Fig. 6C**). Although the OUR measurements were not used to constrain the flux solution, the increases in TCA cycle fluxes (ranging from 2-to 4-fold) determined by MFA also agreed with the observed increases in OUR (**Fig. 5**). Therefore, the MFA results provide further evidence of global upregulation of oxidative metabolism in the PGC-1 α expressing pools.

Pyruvate fluxes were previously found to vary strongly in response to shifts in oxidative metabolic capacity (Templeton et al., 2014). Although total pyruvate flux increased in the PGC- 1α pools, the percentage contribution via pyruvate kinase (PK) was consistent across all cell lines, regardless of PGC- 1α overexpression (**Fig. 8A**). The percentage of pyruvate consumed by pyruvate dehydrogenase (PDH), the major pyruvate sink and primary route of carbon entry to the TCA cycle, was also not significantly different between the parental line and the PGC- 1α expressing pools (**Fig. 8B**). This observation suggests that energy metabolism was elevated at a global level in PGC- 1α expressing pools, as opposed to a local redistribution of fluxes surrounding the pyruvate branch point.

4 Discussion

PGC-1 α is a transcriptional co-activator that globally regulates mitochondrial metabolism in a variety of tissues (Rodgers et al., 2008). PGC-1 α controls mitochondrial biogenesis and remodeling, regulates cellular respiration via the expression of cytochrome c oxidase and electron transport chain components (**Fig. 1**), and performs other tissue-specific functions (Austin and St-Pierre, 2012; Chan and Arany, 2014; Puigserver and Spiegelman, 2003; Scarpulla, 2011). In muscle, PGC-1 α regulates oxidative phosphorylation and increases glucose uptake (Chan and Arany, 2014; Mootha et al., 2004). In primary hepatocytes, PGC-1 α increases mitochondrial DNA content as well as the expression of citrate synthase and electron transport chain proteins (Matthew Morris et al., 2012). Additionally, PGC-1 α is an important regulator of gluconeogenesis in the liver (Chang et al., 2016; Felder et al., 2011; Yoon et al., 2001). In cardiac myocytes, PGC-1 α overexpression increases the expression of genes involved in energy-production pathways, cellular mitochondrial content, and oxygen consumption (Lehman et al., 2000). Knockout of PGC-1 α in cardiac tissue lowers cellular ATP levels and ATP production per mole of oxygen consumed, indicating lower respiratory efficiency (Lehman et al., 2008). Overall, the role of PGC-1 α in metabolism has been well characterized in a variety of different tissue and cell types but has not been examined in CHO cells.

In light of the extensive effects PGC-1α has on metabolism in other cell types, our study sought to assess the extent to which PGC-1α overexpression would enhance oxidative metabolism in an industrial CHO cell line and whether these metabolic alterations would correlate with increased qP. Previous studies have identified an association between high-producing CHO cell lines and elevated mitochondrial metabolism (Templeton et al., 2017a, 2013; Templeton and Young, 2018). It has been shown that increasing pyruvate dehydrogenase (PDH) activity, which directs pyruvate into the TCA cycle, by inhibiting PDH kinase activity leads to increased mAb titers (Buchsteiner et al., 2018; Zhou et al., 2011). Overexpression of the mitochondrial pyruvate carrier (MPC) or yeast pyruvate carboxylase (PYC2) was shown to enhance mitochondrial metabolism and specific mAb productivity in CHO cells (Bulté et al., 2020; Gupta et al., 2017). Knockout of the pyruvate kinase muscle (PKM) isoform also leads to increased specific productivity, alongside reduced lactate production and increased TCA cycle flux (Tang et al., 2021). Furthermore, transfection of CHO cells with the microRNA miR-31* increased oxidative phosphorylation and enhanced mAb specific productivity (Martinez-lopez et al., 2021).

A selection strategy to enrich CHO host populations with cells exhibiting enhanced mitochondrial membrane potential was found to increase the abundance of high-producing clones after stable transfection to secrete difficult-to-express bispecific antibodies (Chakrabarti et al., 2022). These studies support our hypothesis that enhancing mitochondrial metabolism of CHO host cells can promote improved mAb titer and qP. To our knowledge, our study is the first to evaluate the phenotypes of CHO cells that have been rationally engineered to increase oxidative metabolism by overexpressing a global regulator of mitochondrial metabolism.

All three PGC-1 α expressing pools exhibited increased consumption of glucose, lactate, and amino acids. High lactate consumption rates during stationary phase have been correlated to high productivities in CHO cell cultures (Le et al., 2012; Templeton et al., 2017a), a finding corroborated in this study. Higher LURs could prolong culture longevity by removing toxic lactate buildup from the media. Lactate can also serve as an additional carbon source for the TCA cycle upon its conversion to pyruvate. The conversion of lactate to pyruvate by lactate dehydrogenase produces NADH, and it is conjectured that CHO cells switch from lactate production to lactate consumption to replenish the cytosolic pool of NADH when glycolytic rates are slowed (Hartley et al., 2018). The reducing power of cytosolic NADH can indirectly enter the mitochondria through the malate-aspartate shuttle, further fueling oxidative phosphorylation. The observation of both increased lactate consumption as well as increased oxidative metabolism of the PGC-1 α pools supports the hypothesis that higher lactate uptake can fuel the increase in mitochondrial metabolism necessary to sustain high mAb productivities (Hartley et al., 2018).

The three selected PGC-1 α expressing pools exhibited upregulated TCA cycle activity compared to the parental cell line. This increase in TCA cycle flux was directly correlated to the increase in oxygen consumption observed in these stable pools. The measured OURs closely mirrored the trend in oxidative metabolic fluxes and independently confirmed the 13 C MFA results, since the OUR measurements were not used to constrain the flux solution. These increased OURs and TCA cycle fluxes suggest that PGC-1 α has a similar impact on oxidative metabolic capacity and oxygen consumption in CHO cells that has been reported in other types of mammalian cells (Lehman et al., 2000; Wu et al., 1999).

While increased oxidative metabolism was previously found to correlate with increased qP in CHO cells, it has remained an open question whether the increase in qP was a cause or an effect of metabolic alterations within the host. Here, we show that CHO cells specifically engineered to upregulate oxidative metabolism exhibit enhanced qP, supporting the hypothesis that increased oxidative capacity may promote higher mAb production. These findings also further establish that high-producing CHO cell lines (i.e., with qP > ~20 pg/cell/day) require a highly active TCA cycle to support the energy demands of product biosynthesis and secretion. On the other hand, correlations between qP and TCA cycle flux may not hold in low-producing cell lines because factors other than energetics likely limit product formation in those cells (Sacco et al., 2022). Our results also indicate an inherent trade-off between mAb production and growth, as evidenced by the significantly decreased growth rates and peak VCDs, and increased cell size, observed in the PGC-1α overexpressing pools. The correlation of increased cell size with increased specific productivity has been previously reported (Feary et al., 2017; Lloyd et al., 2000; Pan et al., 2017; Wijaya et al., 2021). Additionally, the inverse correlation between cellular growth rate and productivity has been widely observed (Wilkens and Gerdtzen, 2015; Wolf et al., 2019; Zou et al., 2018). These results highlight that total protein production (for both biomass and mAb) needs to be considered when optimizing metabolism to achieve maximum product titers (Templeton et al., 2017b).

The data presented herein supports the hypothesis that highly active mitochondrial metabolism is required for maximal qP in CHO cells. However, the study has some inherent limitations that could influence the interpretation of these results. First, the shake flask cultures used to characterize the cell lines in this study may not reflect their performance in controlled, stirred-tank bioreactors. Second, the selection process used to obtain stable pools could have impacted the outcome of the study. Initial pools were selected based on rapid growth in the presence of zeocin. Given the observed decrease in growth rate of the PGC-1α pools relative to the parental line, the initial selection could have failed to recover stable pools with even higher qP levels due to poor cell growth. Third, the three pools selected for in-depth characterization were chosen based on a screen to identify cell lines with increased qP relative to the parental line, which introduced another source of potential bias. However, the parental cell line had already undergone multiple rounds of selection and screening at Janssen prior to this study and therefore was representative of a highly optimized production cell line.

Furthermore, the selection process used to obtain stable PGC- 1α pools is not altogether different from the process used in industry to identify lead production cell lines, where large numbers of clones are generated and screened based on their relative production levels. If the integration of PGC- 1α had no effect, the resulting stable pools would be expected to have both higher and lower qP relative to the parental line. In fact, given that we only examined 12 stable pools, it is somewhat remarkable that we identified three with substantially elevated qP compared to the parental line and that all stable pools had qP values that were at least as high as the parental line (**Fig. 2A**).

In addition to the potential biases introduced by the selection process, clonal variation is a widely reported observation in CHO cells (Bandyopadhyay et al., 2019; Ghorbaniaghdam et al., 2014; Lee et al., 2018). In this study, random chromosomal integration was used to generate the PGC-1 α expressing mini-pools. Due to the inherent genomic variation of CHO cells, the integration site has a strong effect on the expression of the transgene and possibly other endogenous genes nearby (Lee et al., 2019). Even in daughter clones generated from a single stable clone, a variety of different phenotypes have been observed due to the plasticity of the CHO genome (Ko et al., 2018). In light of the poorly understood effects of clonal variation, the emergence of metabolic phenotypes that are not directly due to PGC-1 α expression remains a possibility. However, the use of stable pools rather than single-cell clones tends to average these random effects over a larger population of cells and thereby minimizes the chances that clonal variation would mask the impact of PGC-1 α in our study.

This study tested the hypothesis that increased mitochondrial metabolism promotes elevated product qP in CHO cell lines. Overexpressing the global mitochondrial regulator PGC-1 α in an industrial IgG-secreting parental line led to selection of stable pools with increased qP, OUR, and energy-producing metabolic fluxes. Both glucose and lactate consumption were elevated by PGC-1 α overexpression. Interestingly, metabolism was upregulated throughout glycolysis and TCA cycle pathways without repartitioning flux around pyruvate or other major branch points. While decreased growth was apparent in the PGC-1 α expressing stable pools, volumetric titers were still increased due the dramatic increase in qP. Overall, this study highlights the potential of host cell engineering to optimize the metabolic phenotypes of CHO cell lines for efficient biomanufacturing.

5 Acknowledgments

This study was supported by the National Science Foundation (NSF) GOALI Program (Grant numbers CBET-1604426, CBET-2035085) and NSF Graduate Research Fellowship Program (Grant numbers 1445197, 1937963). Any opinions, findings, and conclusions or recommendations expressed in this material are those of the author(s) and do not necessarily reflect the views of the National Science Foundation.

6 References

- Amat, R., Planavila, A., Chen, S.L., Iglesias, R., Giralt, M., Villarroya, F., 2009. SIRT1 controls the transcription of the peroxisome proliferator-activated receptor-γ co-activator-1α(PGC-1α) gene in skeletal muscle through the PGC-1α autoregulatory loop and interaction with MyoD. J. Biol. Chem. 284, 21872–21880. https://doi.org/10.1074/jbc.M109.022749
- Antoniewicz, M.R., 2020. A guide to metabolic flux analysis in metabolic engineering: Methods, tools and applications. Metab. Eng. 63, 2–12. https://doi.org/10.1016/j.ymben.2020.11.002
- Antoniewicz, M.R., Kelleher, J.K., Stephanopoulos, G., 2011. Measuring deuterium enrichment of glucose hydrogen atoms by gas chromatography/mass spectrometry. Anal. Chem. 83, 3211–3216. https://doi.org/10.1021/ac200012p
- Austin, S., St-Pierre, J., 2012. PGC1α and mitochondrial metabolism--emerging concepts and relevance in ageing and neurodegenerative disorders. J. Cell Sci. 125, 4963–4971. https://doi.org/10.1242/jcs.113662
- Bandyopadhyay, A.A., O'Brien, S.A., Zhao, L., Fu, H.Y., Vishwanathan, N., Hu, W.S., 2019. Recurring genomic structural variation leads to clonal instability and loss of productivity. Biotechnol. Bioeng. 116, 41–53. https://doi.org/10.1002/bit.26823
- Becker, J., Hackl, M., Rupp, O., Jakobi, T., Schneider, J., Szczepanowski, R., Bekel, T., Borth, N., Goesmann, A., Grillari, J., Kaltschmidt, C., Noll, T., Pühler, A., Tauch, A., Brinkrolf, K., 2011. Unraveling the Chinese hamster ovary cell line transcriptome by next-generation sequencing. J. Biotechnol. 156, 227–235. https://doi.org/10.1016/j.jbiotec.2011.09.014
- Buchsteiner, M., Quek, L.E., Gray, P., Nielsen, L.K., 2018. Improving culture performance and antibody production in CHO cell culture processes by reducing the Warburg effect. Biotechnol. Bioeng. 115, 2315–2327. https://doi.org/10.1002/bit.26724
- Bulté, D.B., Palomares, L.A., Parra, C.G., Martínez, J.A., Contreras, M.A., Noriega, L.G., Ramírez, O.T., 2020. Overexpression of the mitochondrial pyruvate carrier reduces lactate production and increases recombinant protein productivity in CHO cells. Biotechnol. Bioeng. 117, 2633–2647. https://doi.org/10.1002/bit.27439
- Carrier, J.C., Deblois, G., Champigny, C., Levy, E., Giguère, V., 2004. Estrogen-related receptor α (ERRα) is a transcriptional regulator of apolipoprotein A-IV and controls lipid handling in the intestine. J. Biol. Chem. 279, 52052–52058. https://doi.org/10.1074/jbc.M410337200
- Chakrabarti, L., Chaerkady, R., Wang, J., Weng, S.H.S., Wang, C., Qian, C., Cazares, L., Hess, S., Amaya, P., Zhu, J., Hatton, D., 2022. Mitochondrial membrane potential-enriched CHO host: a novel and powerful tool for improving biomanufacturing capability. MAbs 14. https://doi.org/10.1080/19420862.2021.2020081
- Chan, M.C., Arany, Z., 2014. The many roles of PGC-1α in muscle Recent developments. Metabolism. 63, 441–451. https://doi.org/10.1016/j.metabol.2014.01.006
- Chang, J.S., Jun, H.-J., Park, M., 2016. Transcriptional coactivator NT-PGC-1α promotes gluconeogenic gene expression and enhances hepatic gluconeogenesis. Physiol. Rep. 4, 1–14. https://doi.org/10.14814/phy2.13013
- Cheah, Y.E., Young, J.D., 2018. Isotopically nonstationary metabolic flux analysis (INST-MFA): putting theory into practice. Curr. Opin. Biotechnol. 54, 80–87. https://doi.org/10.1016/j.copbio.2018.02.013
- Crown, S.B., Antoniewicz, M.R., 2013. Publishing 13C metabolic flux analysis studies: A review and future perspectives. Metab. Eng. 20, 42–48. https://doi.org/10.1016/j.ymben.2013.08.005
- Dorai, H., Yun, S.K., Ellis, D., Kinney, C.A., Lin, C., Jan, D., Moore, G., Betenbaugh, M.J., 2009. Expression of anti-apoptosis genes alters lactate metabolism of Chinese Hamster ovary cells in culture. Biotechnol. Bioeng. 103, 592–608. https://doi.org/10.1002/bit.22269
- Feary, M., Racher, A.J., Young, R.J., Smales, C.M., 2017. Methionine sulfoximine supplementation enhances productivity in GS–CHOK1SV cell lines through glutathione biosynthesis. Biotechnol. Prog. 33, 17–25. https://doi.org/10.1002/btpr.2372

- Felder, T.K., Soyal, S.M., Oberkofler, H., Hahne, P., Auer, S., Weiss, R., Gadermaier, G., Miller, K., Krempler, F., Esterbauer, H., Patsch, W., 2011. Characterization of novel peroxisome proliferator-activated receptor γ coactivator-1α (PGC-1α) isoform in human liver. J. Biol. Chem. 286, 42923–42936. https://doi.org/10.1074/jbc.M111.227496
- Fischer, S., Handrick, R., Otte, K., 2015. The art of CHO cell engineering: A comprehensive retrospect and future perspectives. Biotechnol. Adv. 33, 1878–1896. https://doi.org/10.1016/j.biotechadv.2015.10.015
- Ghorbaniaghdam, A., Chen, J., Henry, O., Jolicoeur, M., 2014. Analyzing clonal variation of monoclonal antibody-producing CHO cell lines using an in silico metabolomic platform. PLoS One 9. https://doi.org/10.1371/journal.pone.0090832
- Gupta, S.K., Srivastava, S.K., Sharma, A., Nalage, V.H.H., Salvi, D., Kushwaha, H., Chitnis, N.B., Shukla, P., 2017. Metabolic engineering of CHO cells for the development of a robust protein production platform. PLoS One 12, e0181455. https://doi.org/10.1371/journal.pone.0181455
- Gutierrez, J.M., Feizi, A., Li, S., Kallehauge, T.B., Hefzi, H., Grav, L.M., Ley, D., Baycin Hizal, D., Betenbaugh, M.J., Voldborg, B., Faustrup Kildegaard, H., Min Lee, G., Palsson, B.O., Nielsen, J., Lewis, N.E., 2020. Genome-scale reconstructions of the mammalian secretory pathway predict metabolic costs and limitations of protein secretion. Nat. Commun. 11, 1–10. https://doi.org/10.1038/s41467-019-13867-y
- Handschin, C., Rhee, J., Lin, J., Tarr, P.T., Spiegelman, B.M., 2003. An autoregulatory loop controls peroxisome proliferator-activated receptor γ coactivator 1α expression in muscle. Proc. Natl. Acad. Sci. U. S. A. 100, 7111–7116. https://doi.org/10.1073/pnas.1232352100
- Hartley, F., Walker, T., Chung, V., Morten, K., 2018. Mechanisms driving the lactate switch in Chinese hamster ovary cells. Biotechnol. Bioeng. 115, 1890–1903. https://doi.org/10.1002/bit.26603
- Ichida, M., Nemoto, S., Finkel, T., 2002. Identification of a specific molecular repressor of the peroxisome proliferator-activated receptor γ coactivator-1 α (PGC-1 α). J. Biol. Chem. 277, 50991–50995. https://doi.org/10.1074/jbc.M210262200
- Jayapal, K.P., Wlaschin, K.F., Hu, W.S., Yap, M.G.S., 2007. Recombinant protein therapeutics from CHO Cells 20 years and counting. Chem. Eng. Prog. 103, 40–47.
- Ko, P., Misaghi, S., Hu, Z., Zhan, D., Tsukuda, J., Yim, M., Sanford, M., Shaw, D., Shiratori, M., Snedecor, B., Laird, M., Shen, A., 2018. Probing the importance of clonality: Single cell subcloning of clonally derived CHO cell lines yields widely diverse clones differing in growth, productivity, and product quality. Biotechnol. Prog. 34, 624–634. https://doi.org/10.1002/btpr.2594
- Kuo, C.C., Chiang, A.W., Shamie, I., Samoudi, M., Gutierrez, J.M., Lewis, N.E., 2018. The emerging role of systems biology for engineering protein production in CHO cells. Curr. Opin. Biotechnol. 51, 64–69. https://doi.org/10.1016/j.copbio.2017.11.015
- Lao, M.S., Toth, D., 1997. Effects of ammonium and lactate on growth and metabolism of a recombinant Chinese hamster ovary cell culture. Biotechnol. Prog. 13, 688–691. https://doi.org/10.1021/bp9602360
- Le, H., Kabbur, S., Pollastrini, L., Sun, Z., Mills, K., Johnson, K., Karypis, G., Hu, W.S., 2012. Multivariate analysis of cell culture bioprocess data—Lactate consumption as process indicator. J. Biotechnol. 162, 210–223. https://doi.org/10.1016/j.jbiotec.2012.08.021
- Lee, J.S., Kildegaard, H.F., Lewis, N.E., Lee, G.M., 2019. Mitigating Clonal Variation in Recombinant Mammalian Cell Lines. Trends Biotechnol. 37, 931–942. https://doi.org/10.1016/j.tibtech.2019.02.007
- Lee, J.S., Park, J.H., Ha, T.K., Samoudi, M., Lewis, N.E., Palsson, B.O., Kildegaard, H.F., Lee, G.M., 2018. Revealing Key Determinants of Clonal Variation in Transgene Expression in Recombinant CHO Cells Using Targeted Genome Editing. ACS Synth. Biol. 7, 2867–2878. https://doi.org/10.1021/acssynbio.8b00290
- Lehman, J.J., Boudina, S., Banke, N.H., Sambandam, N., Han, X., Young, D.M., Leone, T.C., Gross, R.W., Lewandowski, E.D., Abel, E.D., Kelly, D.P., 2008. The transcriptional coactivator PGC-1 is essential for maximal and efficient cardiac mitochondrial fatty acid oxidation and lipid homeostasis. AJP Hear. Circ. Physiol. 295, H185–H196. https://doi.org/10.1152/ajpheart.00081.2008

- Lehman, J.J., Medeiros, D.M., Kelly, D.P., Lehman, J.J., Barger, P.M., Kovacs, A., Saffitz, J.E., Medeiros, D.M., Kelly, D.P., 2000. Peroxisome proliferator activated receptor gamma coactivator-1 promotes cardiac mitochondrial biogenesis Find the latest version: promotes cardiac mitochondrial biogenesis. J. Clin. Invest. 106, 847–856.
- Livak, K.J., Schmittgen, T.D., 2001. Analysis of relative gene expression data using real-time quantitative PCR and the 2-ΔΔCT method. Methods 25, 402–408. https://doi.org/10.1006/meth.2001.1262
- Lloyd, D.R., Holmes, P., Jackson, L.P., Emery, A.N., Al-Rubeai, M., 2000. Relationship between cell size, cell cycle and specific recombinant protein productivity. Cytotechnology 34, 59–70. https://doi.org/10.1023/A:1008103730027
- Lustig, Y., Ruas, J.L., Estall, J.L., Lo, J.C., Devarakonda, S., Laznik, D., Choi, J.H., Ono, H., Olsen, J. V, Spiegelman, B.M., 2011. Separation of the gluconeogenic and mitochondrial functions of PGC-1a through S6 kinase. Genes Dev. 1–13. https://doi.org/10.1101/gad.2054711.ln
- Majewska, N.I., Tejada, M.L., Betenbaugh, M.J., Agarwal, N., 2020. N-Glycosylation of IgG and IgG-like recombinant proteins: Why is it important and how can we control it? Annu. Rev. Chem. Biomol. Eng. 11, 1–28. https://doi.org/10.1146/annurev-ch-3-061212-100001
- Martinez-lopez, J.E., Coleman, O., Meleady, P., Clynes, M., 2021. Transfection of miR-31 * boosts oxidative phosphorylation metabolism in the mitochondria and enhances recombinant protein production in Chinese hamster ovary cells. J. Biotechnol. 333, 86–96. https://doi.org/10.1016/j.jbiotec.2021.04.012
- Matthew Morris, E., Meers, G.M.E., Booth, F.W., Fritsche, K.L., Hardin, C.D., Thyfault, J.P., Ibdah, J.A., 2012. Pgc-1α overexpression results in increased hepatic fatty acid oxidation with reduced triacylglycerol accumulation and secretion. Am. J. Physiol. Gastrointest. Liver Physiol. 303, 979–992. https://doi.org/10.1152/ajpgi.00169.2012
- Mcatee, A.G., Templeton, N., Young, J.D., 2014. Role of Chinese hamster ovary central carbon metabolism in controlling the quality of secreted biotherapeutic proteins. Pharm. Bioprocess. 2, 63–74. https://doi.org/10.4155/pbp.13.65
- Mootha, V.K., Handschin, C., Arlow, D., Xie, X., St Pierre, J., Sihag, S., Yang, W., Altshuler, D., Puigserver, P., Patterson, N., Willy, P.J., Schulman, I.G., Heyman, R. a, Lander, E.S., Spiegelman, B.M., 2004. Erralpha and Gabpa/b specify PGC-1alpha-dependent oxidative phosphorylation gene expression that is altered in diabetic muscle. Proc. Natl. Acad. Sci. U. S. A. 101, 6570–6575. https://doi.org/10.1073/pnas.0401401101
- Mulukutla, B.C., Mitchell, J., Geoffroy, P., Harrington, C., Krishnan, M., Kalomeris, T., Morris, C., Zhang, L., Pegman, P., Hiller, G.W., 2019. Metabolic engineering of Chinese hamster ovary cells towards reduced biosynthesis and accumulation of novel growth inhibitors in fed-batch cultures. Metab. Eng. 54, 54–68. https://doi.org/10.1016/j.ymben.2019.03.001
- Murphy, T.A., Young, J.D., 2013. ETA: Robust software for determination of cell specific rates from extracellular time courses. Biotechnol. Bioeng. 110, 1748–1758. https://doi.org/10.1002/bit.24836
- Pan, X., Dalm, C., Wijffels, R.H., Martens, D.E., 2017. Metabolic characterization of a CHO cell size increase phase in fed-batch cultures. Appl. Microbiol. Biotechnol. 101, 8101–8113. https://doi.org/10.1007/s00253-017-8531-y
- Puigserver, P., Spiegelman, B.M., 2003. Peroxisome proliferator-activated receptor-γ coactivator 1α (PGC-1α): Transcriptional coactivator and metabolic regulator. Endocr. Rev. 24, 78–90. https://doi.org/10.1210/er.2002-0012
- Rodgers, J.T., Lerin, C., Gerhart-hines, Z., Puigserver, P., 2008. Metabolic adaptations through the PGC-1 a and SIRT1 pathways. FEBS Lett. 582, 46–53. https://doi.org/10.1016/j.febslet.2007.11.034
- Rodrigues, M.E., Costa, A.R., Henriques, M., Cunnah, P., Melton, D.W., Azeredo, J., Oliveira, R., 2013. Advances and drawbacks of the adaptation to serum-free culture of CHO-K1 cells for monoclonal antibody production. Appl. Biochem. Biotechnol. 169, 1279–1291. https://doi.org/10.1007/s12010-012-0068-z

- Sacco, S.A., Tuckowski, A.M., Trenary, I., Kraft, L., Betenbaugh, M.J., Young, J.D., Smith, K.D., 2022. Attenuation of glutamine synthetase selection marker improves product titer and reduces glutamine overflow in Chinese hamster ovary cells. Biotechnol. Bioeng. https://doi.org/10.1002/bit.28084
- Sacco, S.A., Young, J.D., 2021. 13C metabolic flux analysis in cell line and bioprocess development. Curr. Opin. Chem. Eng. 34. https://doi.org/10.1016/j.coche.2021.100718
- Scarpulla, R.C., 2011. Metabolic control of mitochondrial biogenesis through the PGC-1 family regulatory network. Biochim. Biophys. Acta 1813, 1269–1278. https://doi.org/10.1016/j.bbamcr.2010.09.019.Metabolic
- Schröder, M., Matischak, K., Friedl, P., 2004. Serum- and protein-free media formulations for the Chinese hamster ovary cell line DUKXB11. J. Biotechnol. 108, 279–292. https://doi.org/10.1016/j.jbiotec.2003.12.005
- Seth, G., Hossler, P., Yee, J.C., Hu, W.-S., 2006. Engineering Cells for Cell Culture Bioprocessing-Physiological Fundamentals. Adv Biochem Eng Biotechnol 101, 119–164.
- Shannon, P., Markiel, A., Ozier, O., Baliga, N.S., Wang, J.T., Ramage, D., Amin, N., Schwikowski, B., Ideker, T., 2003. Cytoscape: A Software Environment for Integrated Models of Biomolecular Interaction Networks. Genome Res. 13, 2498–2504. https://doi.org/10.1101/gr.1239303.metabolite
- Sinacore, M.S., Drapeau, D., Adamson, S.R., 2000. Adaptation of Mammalian Cells to Growth in Serum-Free Media. Mol. Biotechnol. 15.
- Tang, D., Sandoval, W., Liu, P., Lam, C., Snedecor, B., Misaghi, S., 2021. Preventing pyruvate kinase muscle expression in Chinese hamster ovary cells curbs lactogenic behavior by altering glycolysis, gating pyruvate generation, and increasing pyruvate flux into the TCA cycle. Biotechnol. Prog. https://doi.org/10.1002/btpr.3193
- Templeton, N., Dean, J., Reddy, P., Young, J.D., 2013. Peak antibody production is associated with increased oxidative metabolism in an industrially relevant fed-batch CHO cell culture. Biotechnol. Bioeng. 110, 2013–2024. https://doi.org/10.1002/bit.24858
- Templeton, N., Lewis, A., Dorai, H., Qian, E.A., Campbell, M.P., Smith, K.D., Lang, S.E., Betenbaugh, M.J., Young, J.D., 2014. The impact of anti-apoptotic gene Bcl-2∆ expression on CHO central metabolism. Metab. Eng. 25, 92–102. https://doi.org/10.1016/j.ymben.2014.06.010
- Templeton, N., Smith, K.D., McAtee-Pereira, A.G., Dorai, H., Betenbaugh, M.J., Lang, S.E., Young, J.D., 2017a. Application of 13C flux analysis to identify high-productivity CHO metabolic phenotypes. Metab. Eng. 43. https://doi.org/10.1016/j.ymben.2017.01.008
- Templeton, N., Xu, S., Roush, D.J., Chen, H., 2017b. 13C metabolic flux analysis identifies limitations to increasing specific productivity in fed-batch and perfusion 44, 126–133. https://doi.org/10.1016/j.ymben.2017.09.010
- Templeton, N., Young, J.D., 2018. Biochemical and metabolic engineering approaches to enhance production of therapeutic proteins in animal cell cultures. Biochem. Eng. J. 136, 40–50. https://doi.org/10.1016/j.bej.2018.04.008
- Walsh, G., 2018. Biopharmaceutical benchmarks 2018. Nat. Biotechnol. 36, 1136–1145. https://doi.org/10.1038/nbt.4305
- Wijaya, A.W., Verhagen, N., Teleki, A., Takors, R., 2021. Compartment-specific 13C metabolic flux analysis reveals boosted NADPH availability coinciding with increased cell-specific productivity for IgG1 producing CHO cells after MTA treatment. Eng. Life Sci. 21, 832–847. https://doi.org/10.1002/elsc.202100057
- Wilkens, C.A., Gerdtzen, Z.P., 2015. Comparative metabolic analysis of CHO cell clones obtained through cell engineering, for IgG productivity, growth and cell longevity. PLoS One 10, 1–15. https://doi.org/10.1371/journal.pone.0119053
- Wolf, M.K.F., Closet, A., Bzowska, M., Bielser, J.M., Souquet, J., Broly, H., Morbidelli, M., 2019. Improved Performance in Mammalian Cell Perfusion Cultures by Growth Inhibition. Biotechnol. J. 14, 1–9. https://doi.org/10.1002/biot.201700722

- Wu, Z., Puigserver, P., Andersson, U., Zhang, C., Adelmant, G., Mootha, V.K., Troy, A., Cinti, S., Lowell, B., Scarpulla, R.C., Spiegelman, B.M., 1999. Mechanisms Controlling Mitochondrial biogenesis and respiration through the thermogenic coactivator PGC-1. Cell 98, 115–124. https://doi.org/10.1109/freq.2001.956373
- Yoon, J.C., Puigserver, P., Chen, G., Donovan, J., Wu, Z., Rhee, J., Adelmant, G., Stafford, J., Kahn, C.R., Granner, D.K., Newgard, C.B., Spiegelman, B.M., 2001. Control of hepatic gluconeogenesis through the transcriptional coactivator PGC-1. Nature 413, 131–138. https://doi.org/10.1038/35093050
- Young, J.D., 2014. INCA: A computational platform for isotopically non-stationary metabolic flux analysis. Bioinformatics 30, 1333–1335. https://doi.org/10.1093/bioinformatics/btu015
- Zhou, M., Crawford, Y., Ng, D., Tung, J., Pynn, A.F.J., Meier, A., Yuk, I.H., Vijayasankaran, N., Leach, K., Joly, J., Snedecor, B., Shen, A., 2011. Decreasing lactate level and increasing antibody production in Chinese Hamster Ovary cells (CHO) by reducing the expression of lactate dehydrogenase and pyruvate dehydrogenase kinases. J. Biotechnol. 153, 27–34. https://doi.org/10.1016/j.jbiotec.2011.03.003
- Zou, W., Edros, R., Al-Rubeai, M., 2018. The relationship of metabolic burden to productivity levels in CHO cell lines. Biotechnol. Appl. Biochem. 65, 173–180. https://doi.org/10.1002/bab.1574

7 Tables and Figures

Table 1. Experimental timeline of ¹³C labeling experiment. Cultures were fed labeled glucose on day 5 such that total glucose carbon would be approximately 70% ¹³C enriched. Days 5-8 are shaded to indicate the presence of ¹³C-glucose in the cell culture media. Cell pellet and media samples were collected for metabolite analysis on days 7 and 8 at the times indicated (t=40, 48, 60, 72 hrs) following the introduction of ¹³C-glucose on day 5 (t=0). Samples for RT-qPCR analysis to measure gene expression levels were collected on days 5 and 7. Live cells were harvested on day 8 to measure the oxygen uptake rate (OUR) as described in *Materials and Methods*.

Day	0	1	2	3	4	5	6	7		8	
						Feed ¹³ C		RT-c	PCR	O	JR
Event	Inoculate			Feed		(t=0)		Cold Quenches		S	
Event	moculate			reeu		DT «DCD		t=40	t=48	t=60	t=72
						RT-qPCR		hrs	hrs	hrs	hrs

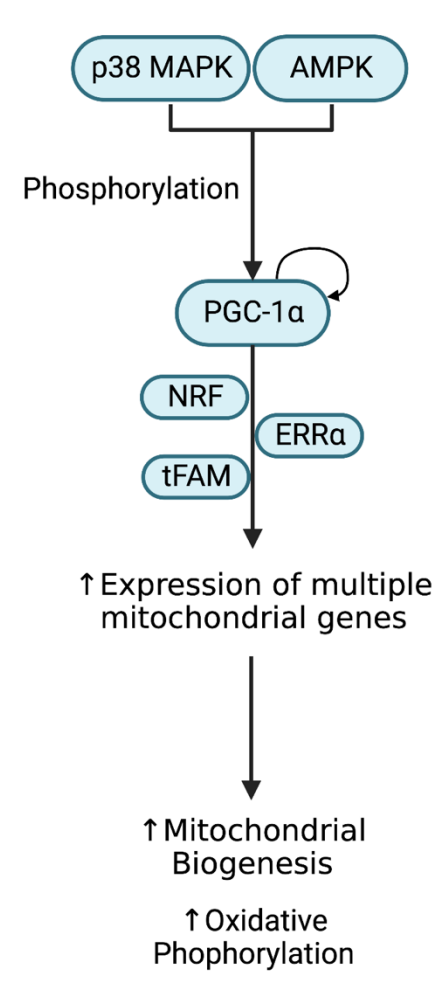


Figure 1. Role of PGC-1 α as a master regulator of mitochondrial biogenesis. PGC-1 α expression is partially controlled by an autoregulatory loop (Handschin et al., 2003). PGC-1 α can be activated via phosphorylation by p38 MAPK and AMPK. Active PGC-1 α , along with transcription factors such as NRF, tFAM, and ERR α , coactivates the expression of multiple mitochondrial genes. This leads to increased mitochondrial biogenesis and increased oxidative phosphorylation. Created with BioRender.com. MAPK, mitogen-activated protein kinase; AMPK, AMP kinase; NRF, nuclear respiratory factor; tFAM, mitochondrial transcription factor A; ERR α , estrogen related receptor alpha.

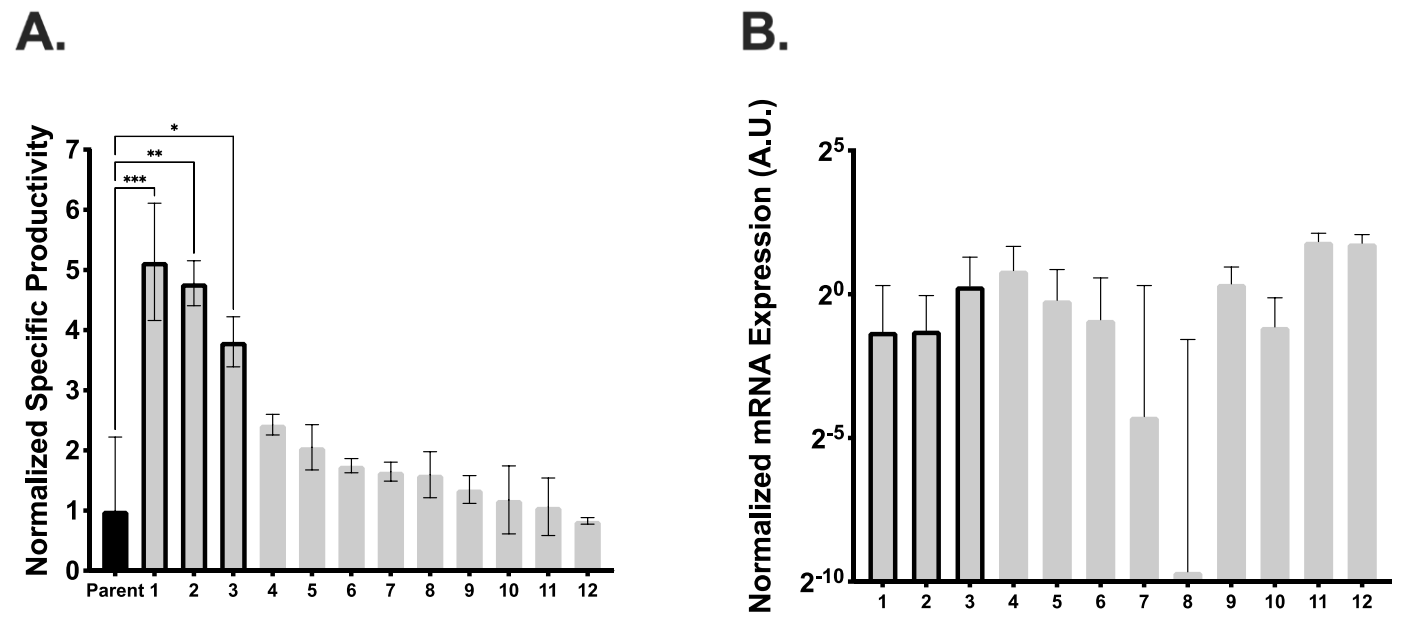


Figure 2. Specific productivity and recombinant PGC-1 α mRNA expression of selected pools. (A) qP was measured for the parental line and 12 PGC-1 α expressing pools. For each pool, qP was normalized to that of the parental line. The three highlighted pools were selected for further evaluation based on their elevated qP values. (B) mRNA expression of recombinant PGC-1 α normalized to HPRT (housekeeping gene) expression as measured by qPCR. All 12 pools exhibited some level of recombinant PGC-1 α mRNA expression; the three pools that were selected for further analysis (bars with black border) had mid-range levels of recombinant PGC-1 α mRNA expression. The parental cell line exhibited no detectable expression of recombinant PGC-1 α , as expected, and is not shown. Data represent mean +/- SEM; * p<0.05, ** p<0.01, *** p<0.01, compared to parental line (n=2).

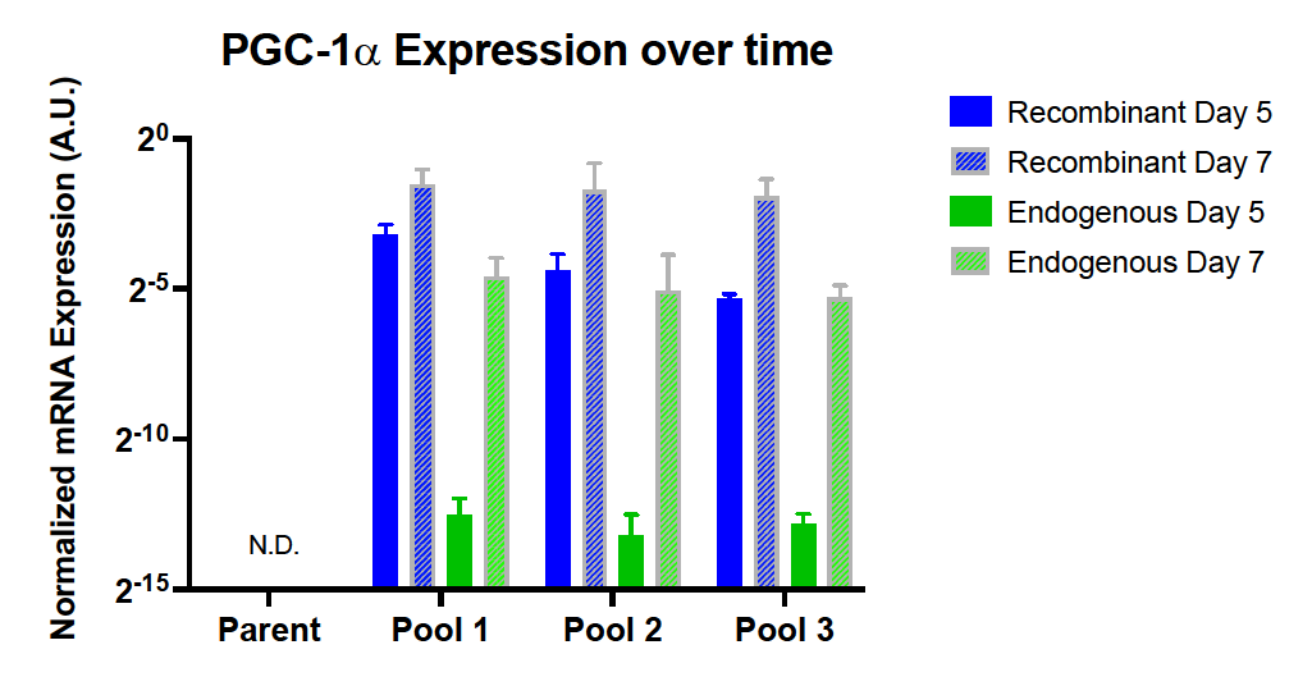


Figure 3. PGC-1 α mRNA expression of selected pools normalized to HPRT expression. The expression levels of both recombinant (human) and endogenous (CHO) PGC-1 α were evaluated on days 5 and 7 of culture for the parental line and three selected pools. No expression of either recombinant or endogenous PGC-1 α was detected in the parental line at either time point. Data represent mean +/- SEM (n=4).

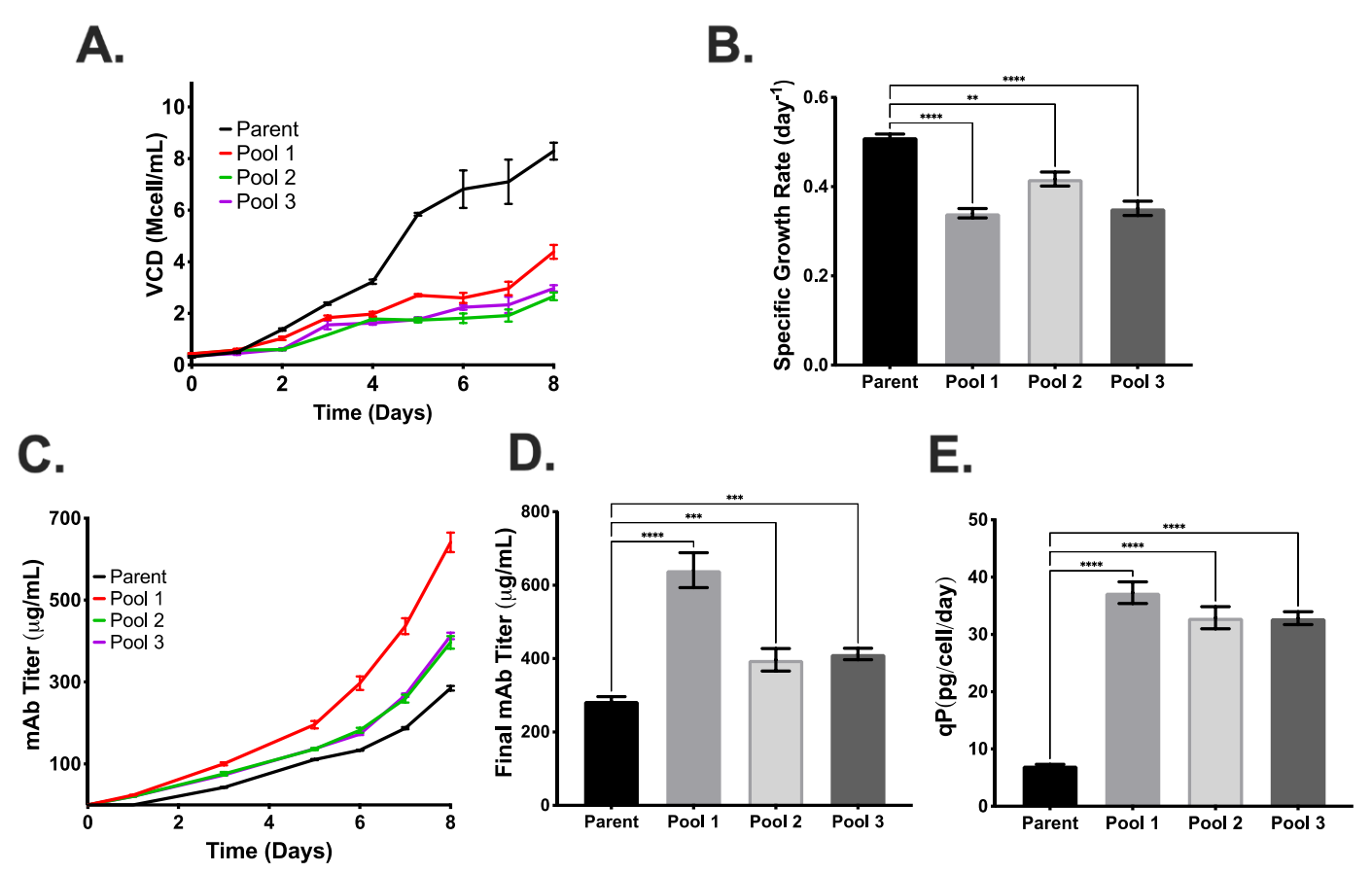


Figure 4. Growth and productivity of the parental line and selected PGC-1 α pools. (A) Viable cell density during the fed-batch study. (B) Specific growth rates during exponential phase. (C) Volumetric titer over the course of the fed-batch study. (D) Final mAb titer measured on day 8 of culture. (E) Specific productivity during the ¹³C labeling experiment. Data represent mean +/- SEM. ** p<0.01, *** p<0.001, **** p<0.0001 compared to the parental line (n=4).

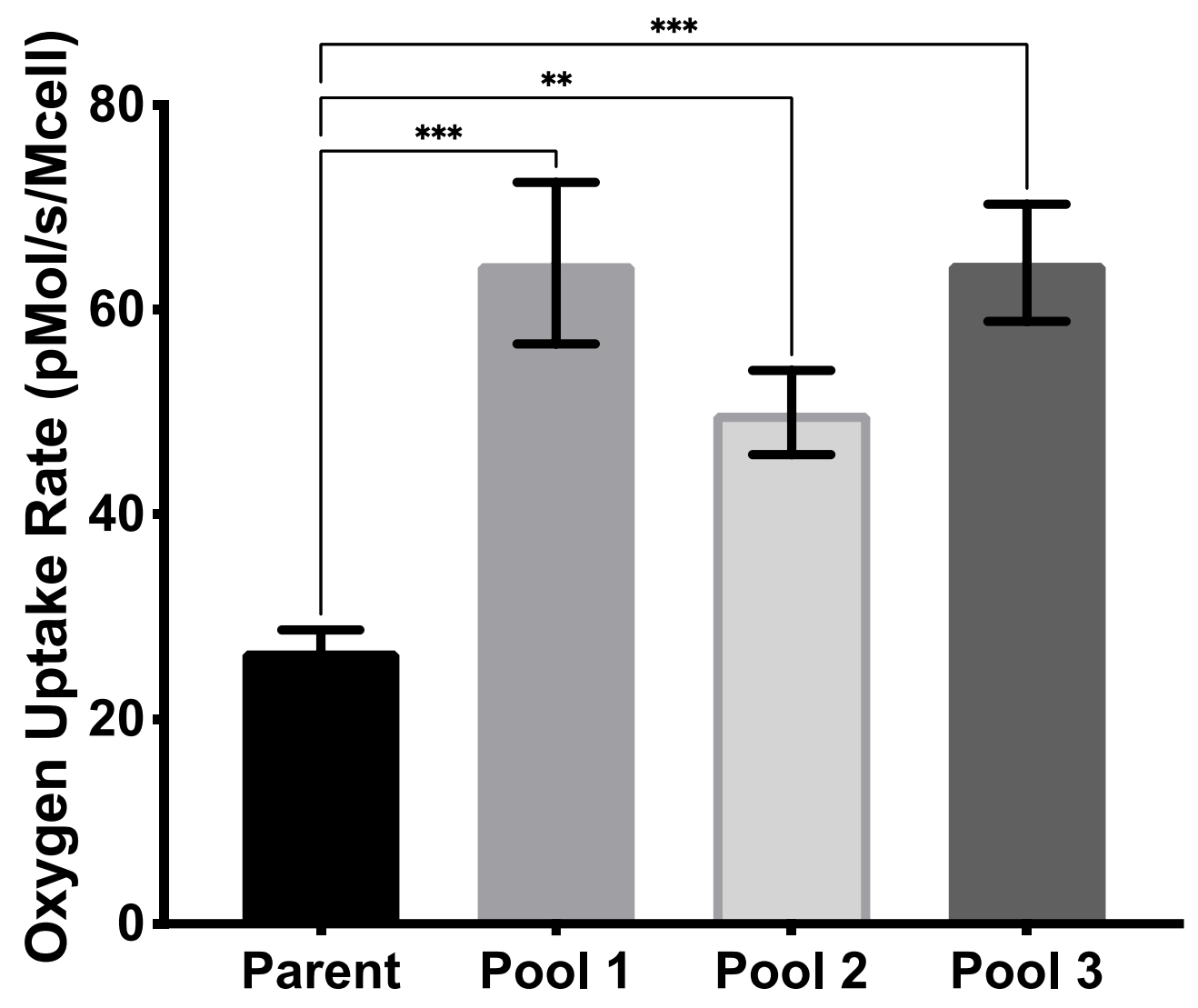


Figure 5. Oxygen uptake rates (OURs) of the parental line and selected PGC-1 α pools. OUR was measured on the final day of culture. Data represent mean +/- SEM. ** p < 0.01, *** p < 0.001, compared to parental line (n=2).

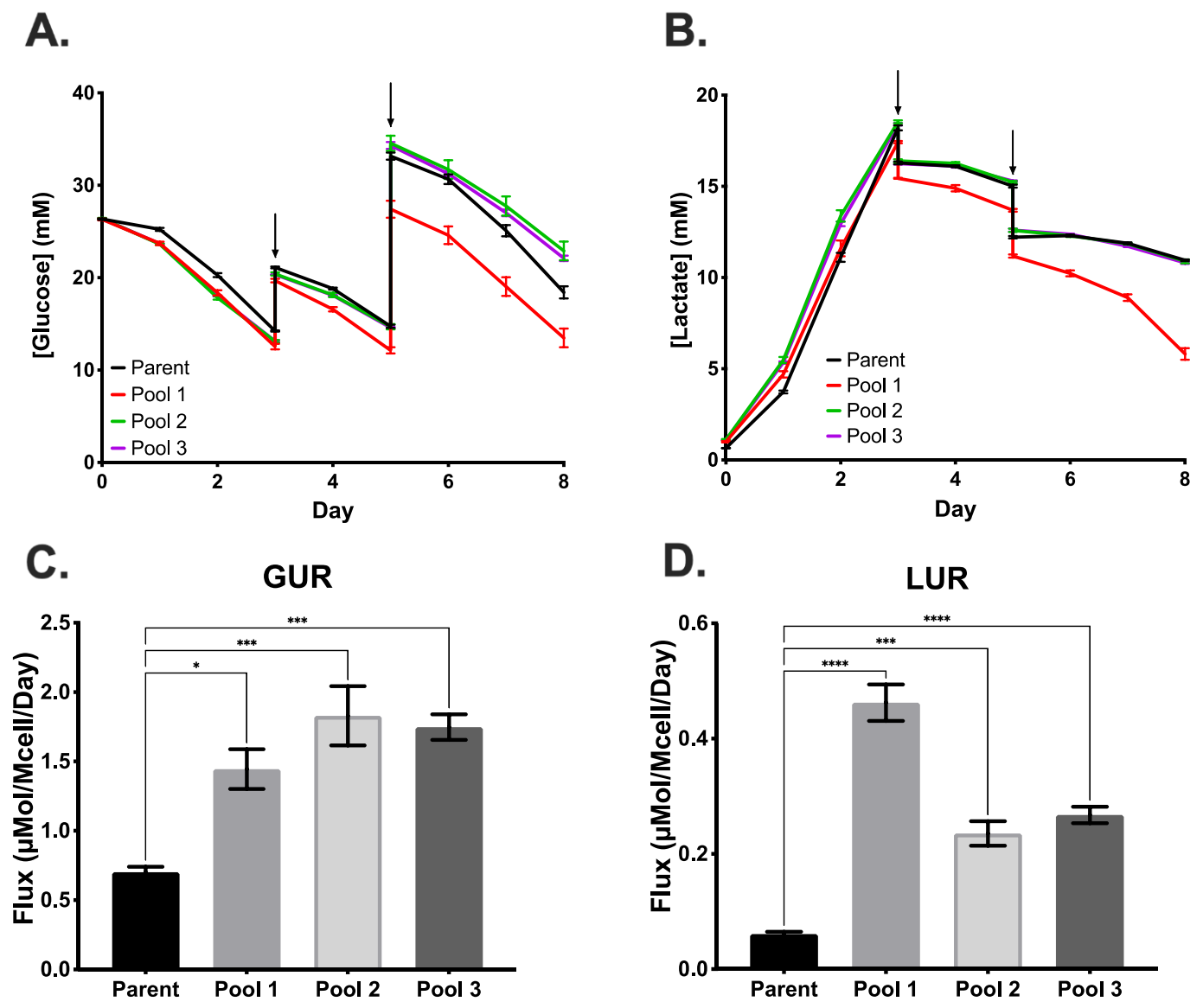


Figure 6. Glucose and lactate consumption rates. (A) Glucose profile over the course of the fed-batch study. (B) Lactate profile over the course of the fed-batch study. (C) Glucose uptake rate (GUR) measured during the 13 C labeling experiment. (D) Lactate uptake rate (LUR) measured during the 13 C labeling experiment. Arrows indicate addition of feed. Data represent mean +/- SEM. ** p<0.01, *** p<0.001, **** p<0.0001 compared to parental line (n=4).

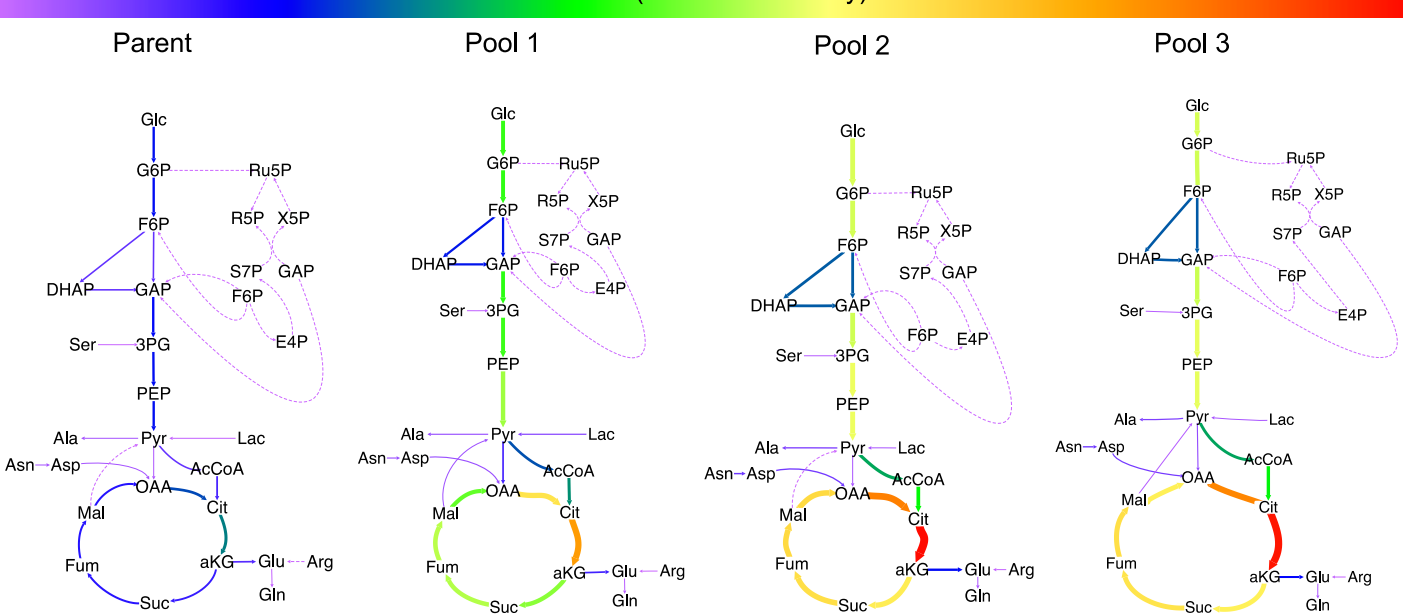


Figure 7. Comparison of metabolic flux maps for the parental line and PGC-1 α expressing pools. Fluxes are shown in units of C-mmol/Mcell/day. The width and color of arrows are scaled to the magnitude of carbon flux. Dotted lines indicate that the flux value was approximately zero (i.e., undetectable).

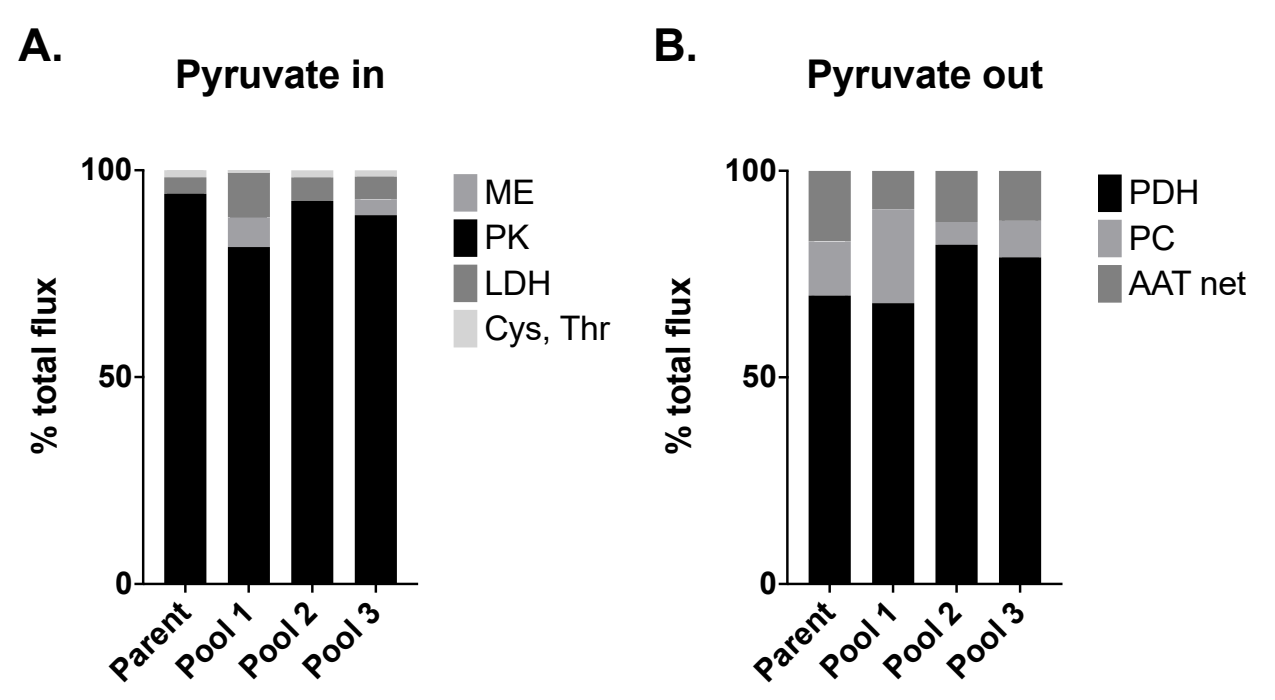


Figure 8. Flux distribution at the pyruvate node. The percent contributions of (A) pyruvate-forming or (B) pyruvate-consuming reactions were calculated based on best-fit fluxes determined by ¹³C MFA. AAT=alanine aminotransferase, Cys=flux from cysteine catabolism, LDH=lactate dehydrogenase, ME=malic enzyme, PC=pyruvate carboxylase, PDH=pyruvate dehydrogenase, PK=pyruvate kinase, Thr=flux from threonine catabolism.

8 Supplementary Material

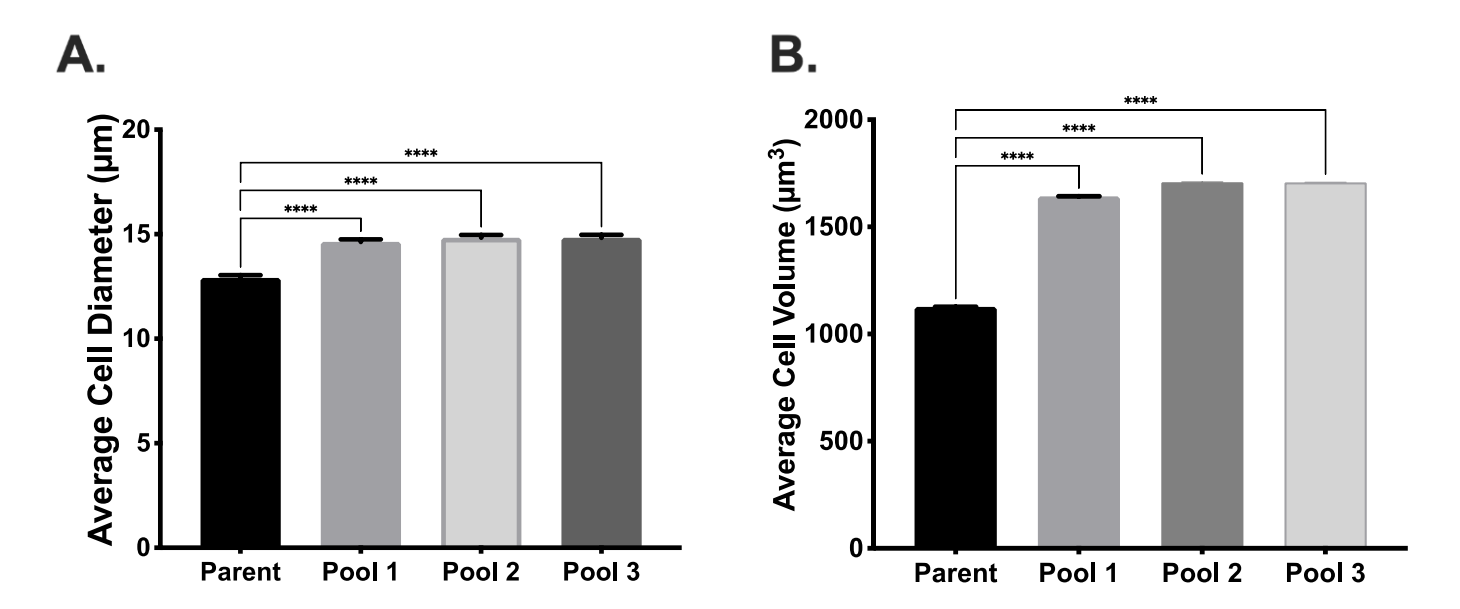


Figure S1. Cell size comparison. (A) Average cell diameter was measured using a Cedex XS automated cell counter. (B) Cell volume was calculated using the measured cell diameter, assuming cells were spherical. Data represent mean +/- SEM. **** indicates statistical significance p < 0.0001, compared to parental line. (n≥7)

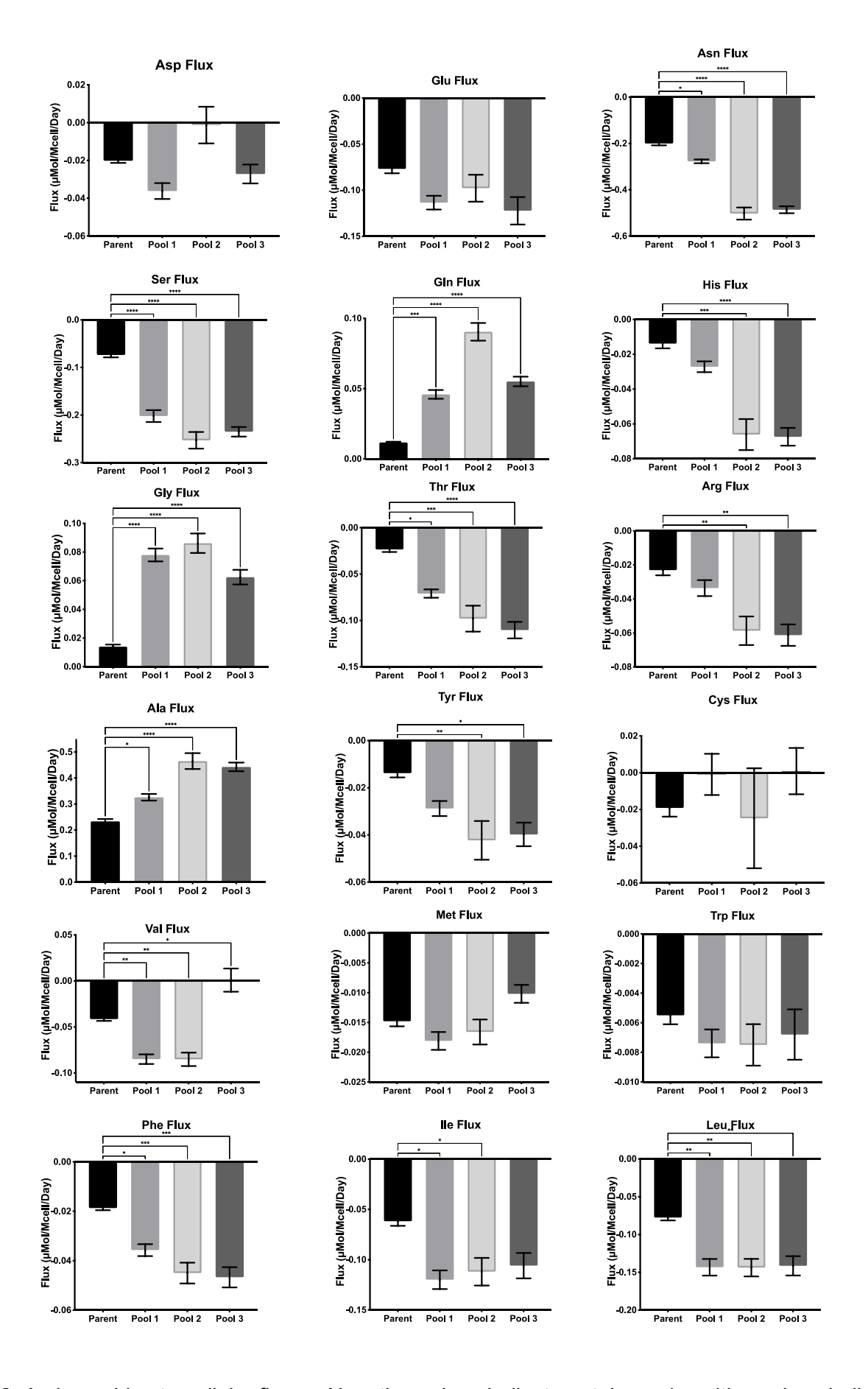


Figure S2. Amino acid extracellular fluxes. Negative values indicate uptake and positive values indicate excretion. Data represent mean +/- SEM. * p < 0.05, ** p < 0.01, *** p < 0.001, compared to parental line (n=4).

Table S1. qPCR primers used for analysis of gene expression.

Gene	Primer Pair
Recombinant (human) PGC-1α	5'-GTCACCACCCAAATCCTTAT-3' (forward)
	5'-ATCTACTGCCTGGAGACCTT-3' (reverse)
Endogenous (CHO) PGC-1α	5'- ACACACCGCAATTCTCCCTT-3' (forward)
	5'- ACGGCGTTCTTCAATTGCTT-3' (reverse)
CHO HPRT	5'- GGACCTCTCGAAGTGTTGGA-3' (forward)
	5'- ATGGGACTCCTCGTGTTTGC-3' (reverse)

Table S2. Model goodness-of-fit metrics as determined by the INCA software. Fits are acceptable if the SSR is below the upper bound of the expected range. SSR=sum-of-squared residuals. DOF=degrees of freedom.

Cell line	Best-fit SSR	SSR expected range	DOF
Parent	142.2	104.7-169.1	135
Pool 1	127.7	85.5-144.3	113
Pool 2	88.7	103.8-167.9	134
Pool 3	79.1	89.8-150.0	118

Table S3. Net fluxes determined by ¹³C MFA for the parental line. Best-fit flux values with 95% confidence intervals indicated by lower bound (LB) and upper bound (UB).

Pathway	Enzyme	Reaction	Net Flux	LB	UB
	HK	Glc ↔ G6P	0.720	0.645	0.797
	PGI	G6P ↔ F6P	0.709	0.469	0.787
	PFK	$F6P \rightarrow DHAP + GAP$	0.704	0.612	0.781
Chrochroid	TPI	$DHAP \leftrightarrow GAP$	0.700	0.605	0.776
Glycolysis	GAPDH	GAP ↔ 3PG	1.401	1.247	1.555
	PGM	3PG ↔ PEP	1.425	1.269	1.580
	PK	$PEP \rightarrow PYR.C$	1.427	1.272	1.678
	LDH	$LAC \leftrightarrow PYR.C$	0.060	0.052	0.068
	G6PDH	$G6P \rightarrow Ru5P$	0.000	0.000	0.243
	PPE	Ru5P ↔ X5P	-0.006	-0.007	0.152
	PPI	Ru5P ↔ R5P	0.006	0.004	0.087
	TKT1	X5P ↔ EC2 + GAP	-0.006	-0.007	0.152
PPP	TKT2	F6P ↔ EC2 + E4P	0.003	-0.076	0.003
	TKT3	S7P ↔ EC2 + R5P	0.003	-0.076	0.003
	TAL1	F6P ↔ EC3 + GAP	0.003	-0.076	0.003
	TAL2	S7P ↔ EC3 + E4P	-0.003	-0.003	0.076
	PDH	Pyr.m → AcCoA.m + CO2	1.041	0.831	1.254
	CS	OAA + AcCoA.m \rightarrow Cit	1.307	1.087	1.526
	IDH.m	Cit ↔ aKG + CO2	1.218	0.992	1.444
TCA Cycle	aKGDH	aKG \rightarrow Suc + CO2	0.746	0.551	1.659
	SDH	Suc ↔ Fum	0.825	0.626	1.737
	FUS	Fum ↔ Mal	0.838	0.639	1.752
	MDH.m	Mal ↔ OAA	0.838	0.486	1.164
	ME	Mal → Pyr.m + CO2	0.000	0.000	1.022
	PC	Pyr.m + CO2 → OAA	0.195	0.079	0.380
Ananlarasia	ATP CS	Cit.c → AcCoa.c + OAA	0.089	0.067	0.110
Anaplerosis	PEPCK	$OAA \rightarrow PEP + CO2$	0.002	-0.080	0.161
	GOT1	$OAA \leftrightarrow Asp$	-0.188	-0.205	-0.171
	Carboxylase	ProCoA + CO2 → Suc	0.078	0.066	0.091
	GS	Gln ↔ Glu	-0.026	-0.029	-0.023
	GluDH	aKG ↔ Glu	0.472	-0.462	0.568
	AsnS	$Asn \to Asp$	-0.187	-0.203	-0.172
	SHMT	Ser ↔ Gly + C1	0.017	0.011	0.023
	PGHDH	$3PG \leftrightarrow Ser$	0.024	0.011	0.037
Amino Acid	GlyS	CO2 + C1 ↔ Gly	0.024	0.021	0.028
Amino Acid Metabolism	ALT	Ala ↔ PYR.c	-0.255	-0.274	-0.237
	Histidase	His \rightarrow C1 + Glu.c	0.007	0.002	0.013
	PAH	$Phe \to Tyr$	0.009	0.006	0.011
	TDO	Trp → CO2 + CO2 + Ala + aKetoadi	0.003	0.002	0.004
	AA Intermediates	aKetoadi → CO2 + CO2 + AcCoA.m + AcCoA.m	0.018	0.005	0.031

	SBCAD	lle → AcCoA.m + CO2 + ProCoA	0.048	0.039	0.058
		Leu + CO2 → CO2 +			
	IVD	AcCoA.m + AcCoA.m + AcCoA.m	0.052	0.043	0.061
	IBD	Val → CO2 + CO2 + ProCoA	0.021	0.016	0.026
	AASS	Lys → aKetoadi	0.015	0.003	0.028
	ARGS	Arg → Glu + Urea	0.008	0.001	0.015
	PO	Glu ↔ Pro	0.521	-0.408	0.624
	CTH	Cys → Pyr	0.022	0.019	0.025
	MAOX	Thr \rightarrow Pyr.m + CO2	0.004	0.000	0.010
	TH	Tyr → CO2 + Fum + AcCoA.m + AcCoA.m	0.013	0.008	0.018
	MAT	Met + Ser → C1 + Cys + ProCoA + Co2	0.009	0.007	0.011
	Glucose	Glc.e → Glc	0.720	0.645	0.797
	Pyr.m	Pyr.c ↔ Pyr.m	1.232	1.073	1.483
	Lys	$Lys.e \to Lys$	0.040	0.029	0.052
	Thr	Thr.e \rightarrow Thr	0.024	0.019	0.029
	Phe	$Phe.e \to Phe$	0.019	0.017	0.020
	Tyr	Tyr.e \rightarrow Tyr	0.014	0.010	0.017
	Val	Val.e → Val	0.042	0.038	0.045
	Leu	Leu.e \rightarrow Leu	0.077	0.070	0.085
	lle	$Ile.e \rightarrow Ile$	0.062	0.053	0.071
	Trp	Trp.e o Trp	0.006	0.004	0.007
	His	$His.e \to His$	0.014	0.008	0.019
Transport	Met	$Met.e \rightarrow Met$	0.015	0.013	0.017
	Ser	$Ser.e \leftrightarrow Ser$	0.074	0.064	0.083
	Ala	Ala ↔ Ala.e	0.233	0.216	0.251
	Arg	Arg.e ↔ Arg	0.023	0.017	0.029
	Asp	$Asp \leftrightarrow Asp.e$	-0.020	-0.022	-0.018
	Cys	$Cys.e \leftrightarrow Cys$	0.019	0.019	0.020
	Glu	Glu ↔ Glu.e	-0.077	-0.086	-0.068
	Gln	Gln ↔ Gln.e	-0.012	-0.013	-0.011
	Gly	$Gly.e \leftrightarrow Gly$	-0.014	-0.017	-0.011
	Pro	$Pro.e \leftrightarrow Pro$	-0.505	-0.610	0.424
	Asn	$Asn.e \leftrightarrow Asn$	0.200	0.185	0.216
	Lac	Lac ↔ Lac.e	-0.060	-0.068	-0.052
		0.033*Ala + 0.016*Cys +			
		0.031*Asp + 0.031*Glu +			
		0.021*Phe + 0.04*Gly +			
Antibody		0.013*His + 0.018*Ile +	0.007	0.004	0.402
Production		0.047*Lys + 0.053*Leu + 0.007*Met + 0.026*Asn +	0.097	0.091	0.103
		0.049*Pro + 0.031*Gln +			
		0.016*Arg + 0.078*Ser +			
		0.059*Thr + 0.058*Val +			

	0.012*Trp + 0.029*Tyr → Antibody			
Biomass Production	0.1776*Ala + 0.1116*Arg + 0.1396*Asp + 0.08529*Asn + 0.04292*Cys + 0.09528*Gln + 0.1143*Glu + 0.1948*Gly + 0.04229*His + 0.09591*Ile + 0.167*Leu + 0.1687*Lys + 0.04085*Met + 0.06487*Phe + 0.09267*Pro + 0.1305*Ser + 0.1143*Thr + 0.01305*Trp + 0.05389*Tyr + 0.1232*Val + 0.08538*G6P + 0.06892*R5P + 0.07548*C1 + 0.03599*DHAP + 0.7326*AcCoA.c -> Biomass	0.121	0.092	0.150

Table S4. Net fluxes determined by 13 C MFA for stable PGC-1 α pool 1. Best-fit flux values with 95% confidence intervals indicated by lower bound (LB) and upper bound (UB).

Pathway	Enzyme	Reaction	Net Flux	LB	UB
	HK	Glc ↔ G6P	1.486	1.232	1.755
	PGI	G6P ↔ F6P	1.474	1.165	1.742
	PFK	$F6P \rightarrow DHAP + GAP$	1.467	1.211	1.737
Chrochroid	TPI	$DHAP \leftrightarrow GAP$	1.462	1.206	1.731
Glycolysis	GAPDH	GAP ↔ 3PG	2.926	2.417	3.463
	PGM	3PG ↔ PEP	3.005	2.494	3.543
	PK	$PEP \rightarrow PYR.C$	3.464	2.467	4.208
	LDH	$LAC \leftrightarrow PYR.C$	0.458	0.397	0.520
	G6PDH	$G6P \rightarrow Ru5P$	0.000	0.000	0.295
	PPE	Ru5P ↔ X5P	-0.007	-0.009	0.158
	PPI	Ru5P ↔ R5P	0.007	0.005	0.105
PPP	TKT1	X5P ↔ EC2 + GAP	-0.007	-0.009	0.158
	TKT2	F6P ↔ EC2 + E4P	0.003	-0.079	0.004
	TKT3	S7P ↔ EC2 + R5P	0.003	-0.079	0.004
	TAL1	F6P ↔ EC3 + GAP	0.003	-0.079	0.004
	TAL2	S7P ↔ EC3 + E4P	-0.003	-0.004	0.079
	PDH	Pyr.m → AcCoA.m + CO2	2.684	2.143	3.360
	CS	OAA + AcCoA.m → Cit	3.180	2.626	3.866
	IDH.m	Cit ↔ aKG + CO2	3.077	2.515	3.767
TCA Cycle	aKGDH	aKG \rightarrow Suc + CO2	2.523	1.815	4.101
_	SDH	$Suc \leftrightarrow Fum$	2.667	1.942	4.247
	FUS	Fum ↔ Mal	2.690	1.987	4.266
	MDH.m	Mal ↔ OAA	2.385	1.551	3.427
	ME	Mal → Pyr.m + CO2	0.304	0.000	1.837
	PC	Pyr.m + $CO2 \rightarrow OAA$	0.897	0.000	1.236
Ananlarasia	ATP CS	Cit.c → AcCoa.c + OAA	0.104	0.072	0.136
Anaplerosis	PEPCK	$OAA \rightarrow PEP + CO2$	0.459	-0.545	0.940
	GOT1	$OAA \leftrightarrow Asp$	-0.253	-0.274	-0.232
	Carboxylase	ProCoA + CO2 → Suc	0.144	0.120	0.169
	GS	Gln ↔ Glu	-0.075	-0.082	-0.068
	GluDH	aKG ↔ Glu	0.554	-0.856	1.081
	AsnS	$Asn \to Asp$	-0.252	-0.269	-0.235
	SHMT	Ser ↔ Gly + C1	0.056	0.047	0.066
	PGHDH	$3PG \leftrightarrow Ser$	0.079	0.051	0.107
	GlyS	CO2 + C1 ↔ Gly	0.069	0.064	0.075
Amino Acid	ALT	Ala ↔ PYR.c	-0.368	-0.394	-0.341
Metabolism	Histidase	$His \rightarrow C1 + Glu.c$	0.015	0.008	0.021
Wictabolisiii	PAH	$Phe \to Tyr$	0.016	0.010	0.022
	TDO	Trp → CO2 + CO2 + Ala + aKetoadi	0.000	0.000	0.001
	AA Intermediates	aKetoadi → CO2 + CO2 + AcCoA.m + AcCoA.m	0.039	0.018	0.060
	SBCAD	lle → AcCoA.m + CO2 + ProCoA	0.097	0.078	0.116

1		Leu + CO2 → CO2 +	I	1	
	IVD	AcCoA.m + AcCoA.m +	0.092	0.069	0.115
	IVD	AcCoA.m	0.032	0.003	0.113
		Val → CO2 + CO2 +			
	IBD	ProCoA	0.038	0.027	0.050
	AASS		0.039	0.018	0.060
		Lys → aKetoadi			
	ARGS	Arg → Glu + Urea	0.010	0.000	0.020
	PO	Glu ↔ Pro	0.585	-0.826	1.122
	CTH	Cys → Pyr	0.000	0.000	0.019
	MAOX	Thr → Pyr.m + CO2	0.026	0.016	0.037
	TH	Tyr \rightarrow CO2 + Fum +	0.023	0.013	0.032
		AcCoA.m + AcCoA.m			
	MAT	Met + Ser → C1 + Cys +	0.009	0.006	0.012
		ProCoA + Co2			
	Glucose	$_{-}^{Glc.e} \to _{-}^{Glc}$	1.486	1.232	1.755
	Pyr.m	Pyr.c ↔ Pyr.m	3.555	2.539	4.311
	Lys	Lys.e → Lys	0.087	0.067	0.107
	Thr	Thr.e \rightarrow Thr	0.072	0.063	0.081
	Phe	Phe.e \rightarrow Phe	0.036	0.031	0.040
	Tyr	Tyr.e → Tyr	0.029	0.022	0.035
	Val	Val.e → Val	0.085	0.075	0.095
	Leu	Leu.e → Leu	0.143	0.121	0.164
	lle	lle.e → lle	0.120	0.101	0.138
	Trp	$Trp.e \to Trp$	0.008	0.007	0.009
	His	His.e → His	0.027	0.021	0.033
Transport	Met	Met.e → Met	0.018	0.015	0.021
	Ser	Ser.e ↔ Ser	0.202	0.177	0.227
	Ala	Ala ↔ Ala.e	0.326	0.301	0.352
	Arg	Arg.e ↔ Arg	0.034	0.024	0.043
	Asp	Asp ↔ Asp.e	-0.036	-0.044	-0.028
	Cys	Cys.e ↔ Cys	0.005	0.000	0.024
	Glu	Glu ↔ Glu.e	-0.114	-0.128	-0.099
	Gln	Glu ↔ Glu.e Gln ↔ Gln.e	-0.114	-0.120	-0.099 -0.040
					-0.040 -0.069
	Gly	Gly.e ↔ Gly	-0.078	-0.087	
	Pro	Pro.e ↔ Pro	-0.547	-1.080	0.867
	Asn	Asn.e ↔ Asn	0.277	0.261	0.293
	Lac	Lac ↔ Lac.e	-0.458	-0.520	-0.397
		0.033*Ala + 0.016*Cys +			
		0.031*Asp + 0.031*Glu +			
		0.021*Phe + 0.04*Gly +			
		0.013*His + 0.018*Ile +			
Antibody		0.047*Lys + 0.053*Leu + 0.007*Met + 0.026*Asn +	0.502	0.454	0.550
Production		0.007"Met + 0.026"Ash + 0.049*Pro + 0.031*Gln +	0.502	0.434	0.550
		0.049 Pro + 0.031 Girl + 0.016*Arg + 0.078*Ser +			
		0.016 Alg + 0.076 Sel + 0.059*Thr + 0.058*Val +			
		$0.039 \text{ Tm} + 0.038 \text{ Val} + 0.012 \text{Trp} + 0.029 \text{Tyr} \rightarrow 0.012 \text{Trp} + 0.029 \text{Tyr} \rightarrow 0.012 \text{Tyr}$			
		Antibody			
		Antibody			

Biomass Production	0.1776*Ala + 0.1116*Arg + 0.1396*Asp + 0.08529*Asn + 0.04292*Cys + 0.09528*Gln + 0.1143*Glu + 0.1948*Gly + 0.04229*His + 0.09591*Ile + 0.167*Leu + 0.1687*Lys + 0.04085*Met + 0.06487*Phe + 0.09267*Pro + 0.1305*Ser + 0.1143*Thr + 0.01305*Trp + 0.05389*Tyr + 0.1232*Val + 0.08538*G6P + 0.06892*R5P + 0.07548*C1 + 0.03599*DHAP + 0.7326*AcCoA.c -> Biomass	0.142	0.098	0.186
-----------------------	--	-------	-------	-------

Table S5. Net fluxes determined by 13 C MFA for stable PGC-1 α pool 2. Best-fit flux values with 95% confidence intervals indicated by lower bound (LB) and upper bound (UB).

Pathway	Enzyme	Reaction	Net Flux	LB	UB
_	HK	Glc ↔ G6P	1.868	1.481	2.278
	PGI	G6P ↔ F6P	1.853	1.443	2.263
	PFK	$F6P \rightarrow DHAP + GAP$	1.846	1.456	2.256
Chroobroio	TPI	$DHAP \leftrightarrow GAP$	1.839	1.450	2.250
Glycolysis	GAPDH	$GAP \leftrightarrow 3PG$	3.681	2.905	4.502
	PGM	3PG ↔ PEP	3.826	3.015	4.647
	PK	$PEP \to PYR.C$	3.826	2.908	4.947
	LDH	$LAC \leftrightarrow PYR.C$	0.235	0.193	0.277
	G6PDH	G6P → Ru5P	0.000	0.000	0.344
	PPE	Ru5P ↔ X5P	-0.008	-0.011	0.176
	PPI	Ru5P ↔ R5P	0.008	0.005	0.100
PPP	TKT1	$X5P \leftrightarrow EC2 + GAP$	-0.008	-0.011	0.176
PPP	TKT2	F6P ↔ EC2 + E4P	0.004	-0.088	0.005
	TKT3	S7P ↔ EC2 + R5P	0.004	-0.088	0.005
	TAL1	F6P ↔ EC3 + GAP	0.004	-0.088	0.005
	TAL2	$S7P \leftrightarrow EC3 + E4P$	-0.004	-0.005	0.088
	PDH	Pyr.m → AcCoA.m + CO2	3.377	2.575	4.398
	CS	OAA + AcCoA.m \rightarrow Cit	4.061	3.239	5.095
	IDH.m	Cit ↔ aKG + CO2	3.937	3.105	4.933
TCA Cycle	aKGDH	aKG \rightarrow Suc + CO2	3.093	2.250	4.673
	SDH	Suc ↔ Fum	3.225	2.379	4.806
	FUS	Fum ↔ Mal	3.269	2.421	4.850
	MDH.m	Mal ↔ OAA	3.269	2.421	4.851
	ME	Mal → Pyr.m + CO2	0.000	0.000	0.679
	PC	Pyr.m + CO2 \rightarrow OAA	0.227	0.000	0.479
Anaplerosis	ATP CS	Cit.c → AcCoa.c + OAA	0.124	0.077	0.170
Anapicrosis	PEPCK	$OAA \rightarrow PEP + CO2$	0.000	-0.386	0.717
	GOT1	$OAA \leftrightarrow Asp$	-0.440	-0.497	-0.384
	Carboxylase	ProCoA + CO2 → Suc	0.132	0.097	0.167
	GS	Gln ↔ Glu	-0.120	-0.134	-0.107
	GluDH	aKG ↔ Glu	0.844	NaN	1.059
	AsnS	$Asn \to Asp$	-0.477	-0.528	-0.425
	SHMT	Ser ↔ Gly + C1	0.045	0.029	0.061
	PGHDH	3PG ↔ Ser	0.145	0.105	0.185
Amino Acid	GlyS	CO2 + C1 ↔ Gly	0.092	0.081	0.103
Metabolism	ALT	Ala ↔ PYR.c	-0.510	-0.571	-0.449
	Histidase	His \rightarrow C1 + Glu.c	0.053	0.036	0.071
	PAH	$Phe \to Tyr$	0.025	0.015	0.034
	TDO	Trp → CO2 + CO2 + Ala + aKetoadi	0.000	0.000	0.003
	AA Intermediates	aKetoadi → CO2 + CO2 + AcCoA.m + AcCoA.m	0.118	0.073	0.163

	SBCAD	lle → AcCoA.m + CO2 + ProCoA	0.087	0.060	0.115
	IV/D	Leu + CO2 → CO2 +	0.004	0.000	0.440
	IVD	AcCoA.m + AcCoA.m + AcCoA.m	0.091	0.066	0.116
	IBD	Val → CO2 + CO2 + ProCoA	0.038	0.022	0.055
	AASS	Lys → aKetoadi	0.118	0.072	0.163
	ARGS	Arg → Glu + Urea	0.033	0.015	0.051
	PO	Glu ↔ Pro	0.874	0.213	1.104
	CTH	Cys → Pyr	0.017	0.000	0.071
	MAOX	Thr \rightarrow Pyr.m + CO2	0.053	0.025	0.082
	TH	Tyr → CO2 + Fum + AcCoA.m + AcCoA.m	0.044	0.025	0.064
	MAT	Met + Ser → C1 + Cys + ProCoA + Co2	0.007	0.002	0.011
	Glucose	Glc.e → Glc	1.868	1.481	2.278
	Pyr.m	Pyr.c ↔ Pyr.m	3.551	2.630	4.674
	Lys	Lys.e → Lys	0.167	0.123	0.212
	Thr	Thr.e \rightarrow Thr	0.099	0.071	0.126
	Phe	Phe.e \rightarrow Phe	0.045	0.037	0.053
	Tyr	Tyr.e → Tyr	0.042	0.026	0.058
	Val	Val.e → Val	0.085	0.071	0.100
	Leu	Leu.e → Leu	0.143	0.120	0.166
	lle	lle.e → lle	0.112	0.085	0.138
	Trp	Trp.e o Trp	0.008	0.007	0.010
	His	His.e → His	0.066	0.049	0.084
Transport	Met	Met.e → Met	0.017	0.013	0.021
	Ser	Ser.e ↔ Ser	0.253	0.219	0.287
	Ala	Ala ↔ Ala.e	0.465	0.405	0.525
	Arg	Arg.e ↔ Arg	0.059	0.042	0.075
	Asp	Asp ↔ Asp.e	-0.001	-0.020	0.018
	Cys	Cys.e ↔ Cys	0.025	0.002	0.078
	Glu	Glu ↔ Glu.e	-0.098	-0.126	-0.069
	Gln	Gln ↔ Gln.e	-0.090	-0.103	-0.078
	Gly	Gly.e ↔ Gly	-0.086	-0.100	-0.073
	Pro	Pro.e ↔ Pro	-0.836	-1.069	NaN
	Asn	Asn.e ↔ Asn	0.503	0.451	0.554
	Lac	Lac ↔ Lac.e	-0.235	-0.277	-0.193
		0.033*Ala + 0.016*Cys +			
		0.031*Asp + 0.031*Glu + 0.021*Phe + 0.04*Gly +			
		0.021 File + 0.04 Gly + 0.013*His + 0.018*Ile +			
Antibody		0.047*Lys + 0.053*Leu +	0.448	0.397	0.499
Production		0.007*Met + 0.026*Asn +			
		0.049*Pro + 0.031*Gln +			
		0.016*Arg + 0.078*Ser +			
		0.059*Thr + 0.058*Val +			

	0.012*Trp + 0.029*Tyr → Antibody			
Biomass Production	0.1776*Ala + 0.1116*Arg + 0.1396*Asp + 0.08529*Asn	0.170	0.105	0.232

Table S6. Net fluxes determined by 13 C MFA for stable PGC-1 α pool 3. Best-fit flux values with 95% confidence intervals indicated by lower bound (LB) and upper bound (UB).

Pathway	Enzyme	Reaction	Net Flux	LB	UB
Glycolysis	HK	Glc ↔ G6P	1.860	1.460	2.279
	PGI	G6P ↔ F6P	1.844	0.445	2.258
	PFK	$F6P \rightarrow DHAP + GAP$	1.835	0.697	2.250
	TPI	$DHAP \leftrightarrow GAP$	1.828	0.688	2.243
	GAPDH	GAP ↔ 3PG	3.659	2.858	4.489
	PGM	3PG ↔ PEP	3.798	2.970	4.657
	PK	$PEP \rightarrow PYR.C$	3.795	2.832	4.655
	LDH	$LAC \leftrightarrow PYR.C$	0.235	0.194	0.277
	G6PDH	G6P → Ru5P	0.000	0.000	3.824
	PPE	Ru5P ↔ X5P	-0.009	-0.017	-0.009
	PPI	Ru5P ↔ R5P	0.009	0.000	1.285
PPP	TKT1	X5P ↔ EC2 + GAP	-0.009	-0.017	-0.009
	TKT2	F6P ↔ EC2 + E4P	0.004	0.004	0.009
	TKT3	S7P ↔ EC2 + R5P	0.004	0.004	0.009
	TAL1	F6P ↔ EC3 + GAP	0.004	0.004	0.009
	TAL2	S7P ↔ EC3 + E4P	-0.004	-0.009	-0.004
	PDH	Pyr.m → AcCoA.m + CO2	3.352	2.466	4.486
	CS	OAA + AcCoA.m → Cit	4.017	3.033	5.295
TCA Cycle	IDH.m	Cit ↔ aKG + CO2	3.877	2.814	5.295
	aKGDH	aKG → Suc + CO2	3.055	2.022	4.661
	SDH	Suc ↔ Fum	3.182	2.123	4.809
	FUS	Fum ↔ Mal	3.224	2.146	4.873
	MDH.m	Mal ↔ OAA	3.064	2.153	4.336
	ME	Mal → Pyr.m + CO2	0.160	0.000	0.872
	PC	Pyr.m + CO2 → OAA	0.375	0.000	0.658
Anaplerosis	ATP CS	Cit.c → AcCoa.c + OAA	0.140	0.000	0.274
	PEPCK	OAA → PEP + CO2	-0.002	-0.483	0.186
	GOT1	$OAA \leftrightarrow Asp$	-0.436	-0.526	-0.364
	Carboxylase	ProCoA + CO2 → Suc	0.127	0.068	0.203
Amino Acid Metabolism	GS	Gln ↔ Glu	-0.122	-0.145	-0.094
	GluDH	aKG ↔ Glu	0.822	0.218	1.209
	AsnS	Asn → Asp	-0.475	-0.536	-0.420
	SHMT	Ser ↔ Gly + C1	0.049	0.006	0.083
	PGHDH	3PG ↔ Ser	0.138	0.074	0.220
	GlyS	CO2 + C1 ↔ Gly	0.092	0.079	0.104
	ALT	Ala ↔ PYR.c	-0.514	-0.584	-0.426
	Histidase	His → C1 + Glu.c	0.052	0.032	0.075
	PAH	$Phe \to Tyr$	0.023	0.008	0.043
	TDO	Trp → CO2 + CO2 + Ala + aKetoadi	0.000	0.000	0.005
	AA Intermediates	aKetoadi → CO2 + CO2 + AcCoA.m + AcCoA.m	0.116	0.060	0.188

	SBCAD	lle → AcCoA.m + CO2 + ProCoA	0.086	0.052	0.127
	IVD	Leu + CO2 → CO2 + AcCoA.m + AcCoA.m +	0.088	0.048	0.140
	IDD	AcCoA.m Val → CO2 + CO2 +	0.000	0.000	0.070
	IBD	ProCoA	0.036	0.008	0.072
	AASS	Lys → aKetoadi	0.116	0.060	0.186
	ARGS	Arg → Glu + Urea	0.030	0.002	0.066
	PO	Glu ↔ Pro	0.844	0.207	1.304
	CTH	Cys → Pyr	0.015	0.000	0.078
	MAOX	Thr \rightarrow Pyr.m + CO2	0.050	0.014	0.095
	TH	Tyr → CO2 + Fum + AcCoA.m + AcCoA.m	0.042	0.012	0.081
	MAT	Met + Ser → C1 + Cys + ProCoA + Co2	0.006	0.000	0.017
	Glucose	Glc.e → Glc	1.860	1.460	2.279
	Pyr.m	Pyr.c ↔ Pyr.m	3.517	2.518	4.415
	Lys —	Lys.e → Lys	0.169	0.124	0.213
	Thr	Thr.e → Thr	0.098	0.070	0.125
	Phe	Phe.e → Phe	0.045	0.037	0.053
	Tyr Val	Tyr.e → Tyr	0.042	0.026	0.058
	vai Leu	Val.e → Val Leu.e → Leu	0.085 0.144	0.071 0.121	0.100 0.166
	lle	lle.e → lle	0.144	0.121	0.100
	Trp	Trp.e \rightarrow Trp	0.112	0.005	0.133
	His	His.e → His	0.066	0.048	0.083
Transport	Met	Met.e → Met	0.017	0.013	0.021
	Ser	Ser.e ↔ Ser	0.253	0.218	0.287
	Ala	Ala ↔ Ala.e	0.465	0.405	0.525
	Arg	Arg.e ↔ Arg	0.059	0.042	0.075
	Asp	Asp ↔ Asp.e	-0.001	-0.020	0.018
	Cys	Cys.e ↔ Cys	0.025	-0.009	0.078
	Glu	Glu ↔ Glu.e	-0.098	-0.126	-0.069
	Gln	Gln ↔ Gln.e	-0.090	-0.103	-0.078
	Gly	Gly.e ↔ Gly	-0.086	-0.100	-0.073
	Pro	Pro.e ↔ Pro	-0.804	-1.283	-0.158
	Asn	Asn.e ↔ Asn	0.503	0.451	0.554
	Lac	Lac ↔ Lac.e	-0.235	-0.277	-0.194
Antibody Production		0.033*Ala + 0.016*Cys + 0.031*Asp + 0.031*Glu + 0.021*Phe + 0.04*Gly + 0.013*His + 0.018*Ile + 0.047*Lys + 0.053*Leu + 0.007*Met + 0.026*Asn +	0.447	0.417	0.477
		0.049*Pro + 0.031*Gln + 0.016*Arg + 0.078*Ser + 0.059*Thr + 0.058*Val +			

	0.012*Trp + 0.029*Tyr → Antibody			
Biomass Production	0.1776*Ala + 0.1116*Arg + 0.1396*Asp + 0.08529*Asn + 0.04292*Cys + 0.09528*Gln + 0.1143*Glu + 0.1948*Gly + 0.04229*His + 0.09591*Ile + 0.167*Leu + 0.1687*Lys + 0.04085*Met + 0.06487*Phe + 0.09267*Pro + 0.1305*Ser + 0.1143*Thr + 0.01305*Trp + 0.05389*Tyr + 0.1232*Val + 0.08538*G6P + 0.06892*R5P + 0.07548*C1 + 0.03599*DHAP + 0.7326*AcCoA.c -> Biomass	0.191	0.000	0.375